Swiss J Geosci (2011) 104:323–343
DOI 10.1007/s00015-011-0068-y

Polyphase movement on the Lavanttal Fault Zone (Eastern Alps): reconciling the evidence from different geochronological indicators

Walter Kurz · Andreas Wölfler · Robert Rabitsch · Johann Genser

Received: 31 January 2011 / Accepted: 24 May 2011 / Published online: 19 August 2011

Abstract The Lavanttal Fault Zone (LFZ) is generally considered to be related to Miocene orogen-parallel escape tectonics in the Eastern Alps. By applying thermochronological methods with retention temperatures ranging from ~450 to ~40°C we have investigated the thermochronological evolution of the LFZ and the adjacent Koralm Complex (Eastern Alps). $^{40}Ar/^{39}Ar$ dating on white mica and zircon fission track (ZFT) thermochronology were carried out on host rocks (HRs) and fault-related rocks (cataclasites and fault gouges) directly adjacent to the unfaulted protolith. These data are interpreted together with recently published apatite fission track (AFT) and apatite (U-Th)/He ages. Sample material was taken from three drill cores transecting the LFZ. Ar release spectra in cataclastic shear zones partly show strongly rejuvenated incremental ages, indicating lattice distortion during cataclastic shearing or hydrothermal alteration. Integrated plateau ages from fault rocks (~76 Ma) are in parts slightly younger than plateau ages from HRs (>80 Ma). Incremental ages from fault rock samples are in part highly reduced (~43 Ma). ZFT ages within fault gouges (~65 Ma) are slightly reduced compared to the ages from HRs, and fission tracks show reduced lengths. Combining these results with AFT and apatite (U-Th)/He ages from fault rocks of the same fault zone allows the recognition of distinct faulting events along the LFZ from Miocene to Pliocene times. Contemporaneous with this faulting, the Koralm Complex experienced accelerated cooling in Late Miocene times. Late-Cretaceous to Palaeogene movement on the LFZ cannot be clearly proven. $^{40}Ar/^{39}Ar$ muscovite and ZFT ages were probably partly thermally affected along the LFZ during Miocene times.

Keywords Major fault zone · Koralm Complex · Austria · Fault rocks · Thermochronology · $^{40}Ar/^{39}Ar$ dating · Zircon fission track dating

1 Introduction

The structure of the Eastern Alps is characterized by a system of fault zones (Fig. 1) resulting from eastward displacement of Austroalpine units during Late Oligocene to Miocene times, described as lateral extrusion by Ratschbacher et al. (1991). Such escape tectonics was responsible for the final exhumation of Penninic and Subpenninic units within tectonic windows (e.g., the Tauern and the Engadine Windows: Selverstone 1988; Genser and Neubauer 1989; Neubauer and Genser 1990; Fügenschuh et al. 1997; Neubauer et al. 2000), and caused the subsidence of sedimentary basins located along the eastern margin of the Eastern Alps (e.g., Styrian Basin; see Fig. 1) and along related strike-slip faults (Figs. 1, 2) (Decker et al. 1993; Decker and Peresson 1996; Wagreich and

Editorial handling: A.G. Milnes.

Electronic supplementary material The online version of this article (doi:10.1007/s00015-011-0068-y) contains supplementary material, which is available to authorized users.

W. Kurz (✉) · A. Wölfler
Institut für Erdwissenschaften, Universität Graz, Heinrichstr. 26, 8010 Graz, Austria
e-mail: walter.kurz@uni-graz.at

R. Rabitsch
Institut für Angewandte Geowissenschaften, Technische Universität Graz, Rechbauerstr. 12, 8010 Graz, Austria

J. Genser
Fachbereich Geographie und Geologie, Universität Salzburg, Hellbrunner Str. 34, 5020 Salzburg, Austria

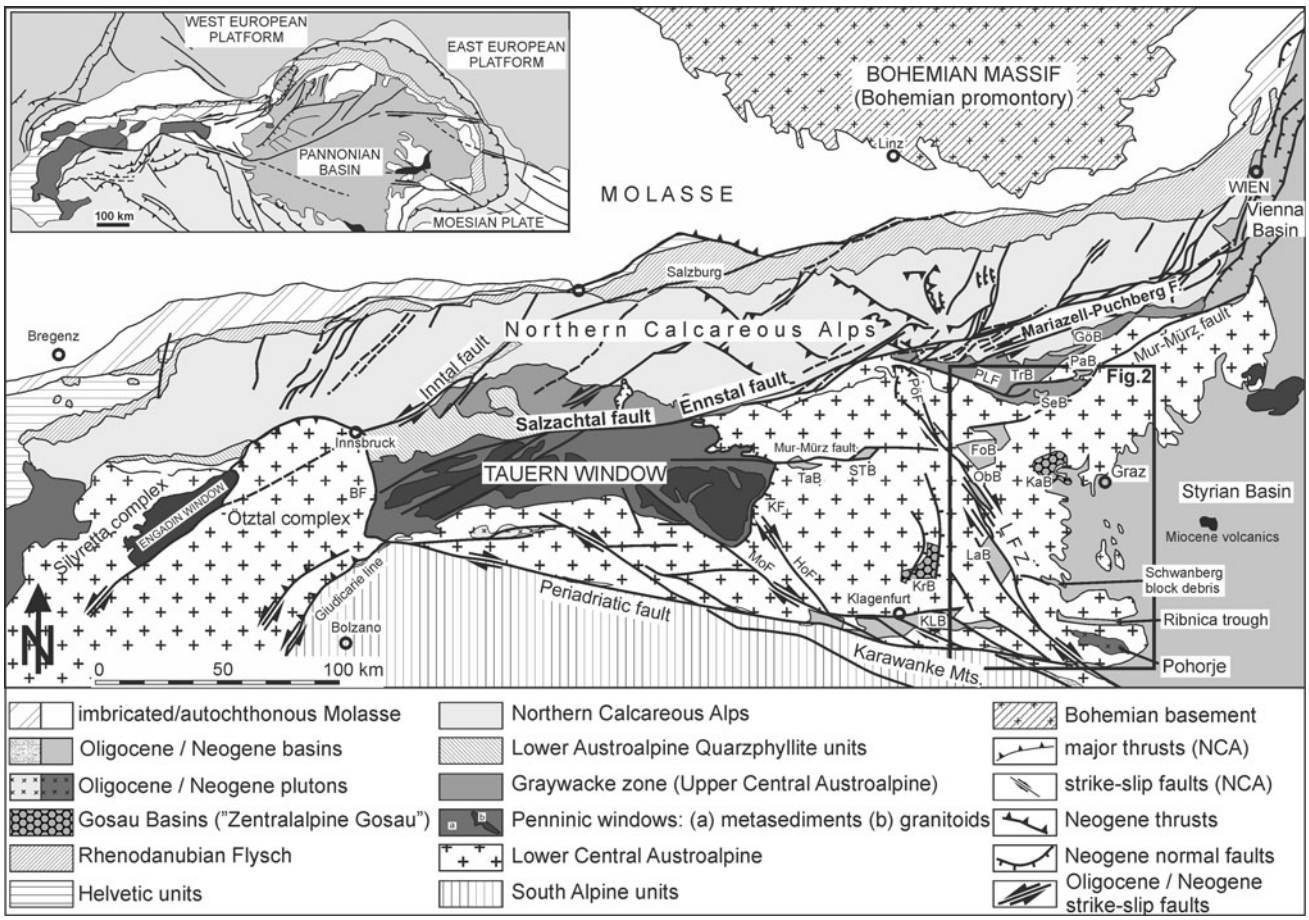

Fig. 1 Tectonic map of the Eastern Alps including Palaeogene to Neogene fault systems. *BF* Brenner normal fault; *HoF* Hochstuhl fault; *KF* Katschberg normal fault; *LFZ* Lavanttal Fault Zone; *MoF* Mölltal fault; *PLF* Palten-Liesing fault; *PöF* Pöls fault (northern part of the LFZ). *FoB* Fohnsdorf Basin; *GöB* Göriach Basin; *KaB* Kainach Basin (Gosau); *KLB* Klagenfurt Basin; *KrB* Krappfeld Basin (Gosau); *LaB* Lavanttal Basin; *ObB* Obdach Basin; *PaB* Parschlug Basin; *SeB* Seegraben Basin; *STB* Seetal Basin; *TaB* Tamsweg Basin; *TrB* Trofaiach Basin

Schmid 2002). Geochronological data from related fault zones are rare and are only available from exhumed faults and mylonitic shear zones in the vicinity of the Tauern Window (Müller et al. 2000, 2001, 2002; Mancktelow et al. 2001). The pseudotachylite ages from these studies are directly dating seismic events along these faults. Dating of fault zones would therefore help to constrain the process of extrusion in time. Constraints are given by pull-apart basins filled with intramontane molasse deposits. Sedimentation within these intramontane basins started at ~18 Ma (e.g., Sachsenhofer et al. 2000).

Another time constraint is given by the exhumation and cooling of Penninic and Subpenninic units in the Tauern Window. White mica $^{40}Ar/^{39}Ar$ ages (e.g., Cliff et al. 1985; Reddy et al. 1993) indicate exhumation-related cooling at 23.5 Ma (Frisch et al. 2000). Within and around the Tauern Window, Müller et al. (2001) and Glodny et al. (2008) demonstrated two peaks of deformation ages, one in the Oligocene between 32 and 30 Ma and a second in the Early to Middle Miocene between 21 and 15 Ma. Ages from pseudotachylites in the southwestern part of the Eastern Alps indicate a period of enhanced fault activity between 22 and 16 Ma (Mancktelow et al. 2001; Müller et al. 2001). Farther east, however, only the upper crustal sections, affected by cataclastic deformation mechanisms, are exposed. Geochronological data from these cataclastic shear zones are rare (e.g., Wölfler et al. 2010). Although the existing reconstructions indicate that the main part of orogen-parallel extension occurred during Early to Middle Miocene times (Frisch et al. 2000), seismic events along most of these faults indicate that these are still active (e.g., Reinecker and Lenhardt 1999; Reinecker 2000; Lenhardt et al. 2007; Frost et al. 2009) and that a certain amount of displacement has been accommodated until recent times.

From geochronological and tectono-metamorphic arguments there is strong evidence that orogen-parallel

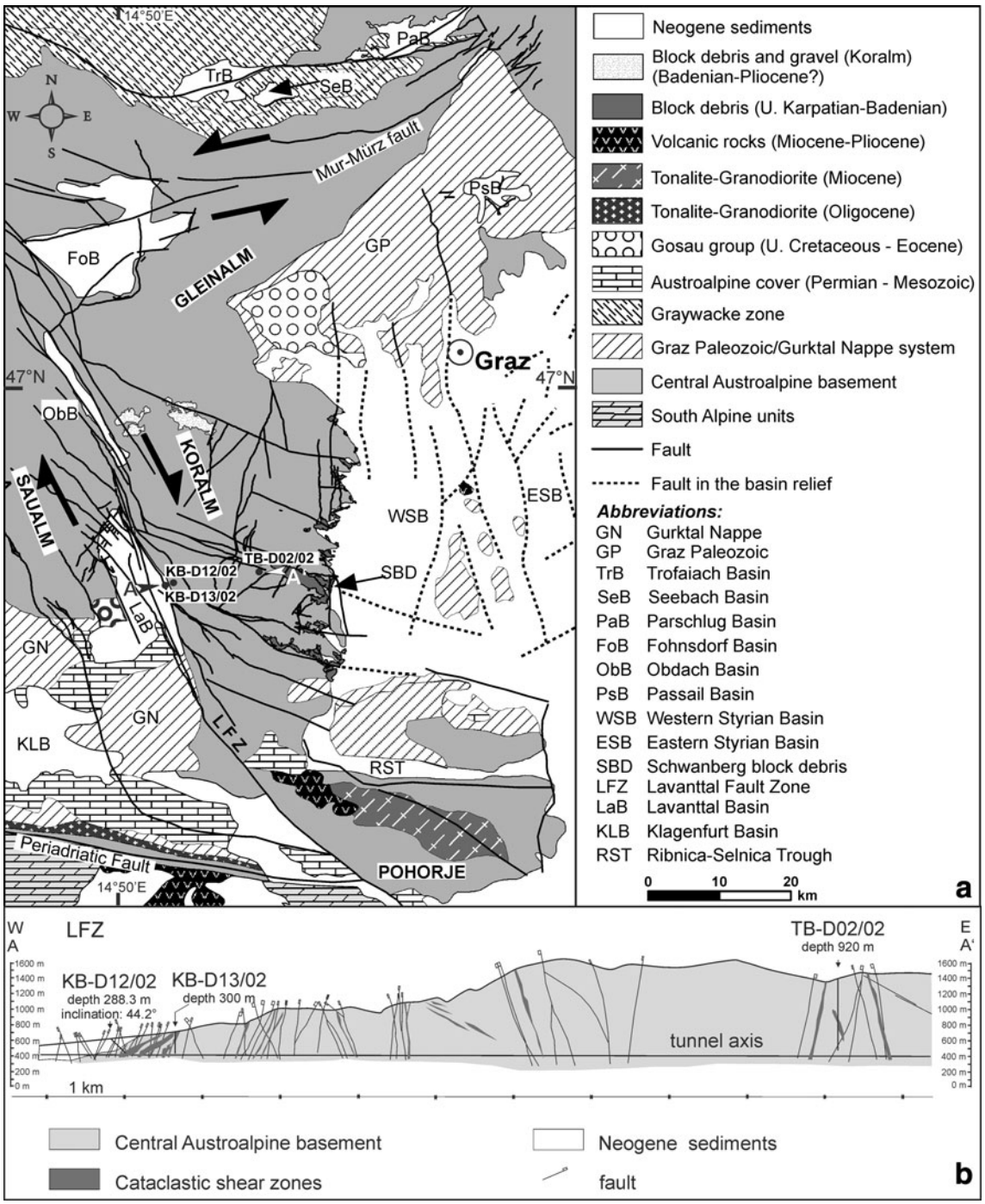

Fig. 2 **a** Geological map of the LFZ including related faults, the Koralm Massif, and adjacent areas (modified after Pischinger et al. 2008; Wölfler et al. 2010). The sampled drilling sites are marked. *A*–*A*′ trace of cross section in Fig. 1b. **b** Simplified geological cross section across the western part of the Koralm massif and the LFZ including faults and cataclastic shear zones documented during surface mapping and drilling campaigns (by courtesy of OeBB, Infrastruktur-Bau)

displacement also played a major role in Alpine tectonics during Late Cretaceous and Palaeogene times (Kurz and Fritz 2003). In particular major fault zones, interpreted as Early Cretaceous thrusts, were overprinted and sealed by upper greenschist- to amphibolite-facies metamorphism, and large rock volumes within the eastern sectors of the Eastern Alps cooled down below 300°C already during Late Cretaceous times (e.g. Hejl 1997, 1998; Fügenschuh et al. 2000). Additionally, a large number of age data previously interpreted to date early Alpine nappe stacking

cluster around 80 Ma and may also be re-interpreted in terms of extension tectonics (for summary, see Kurz and Fritz 2003).

In this study we describe the temporal evolution of the Lavanttal Fault Zone (LFZ, Fig. 2) by the application of thermochronological systems with distinct closure temperature and partial retention zones. The LFZ is located in the easternmost part of the Eastern Alps and is assumed to be related to the Miocene tectonic evolution of the Eastern Alps (Ratschbacher et al. 1991; Frisch et al. 2000; Reinecker 2000). This fault zone is one of the most accessible fault zones in the Eastern Alps thanks to underground excavation and cored drillings related to the geological site investigations for a major railway project in Austria (Koralm base tunnel). Structural data document multiple deformation events (Pischinger et al. 2008). Thermochronological data presented in this study show that distinct faulting events were accompanied by thermal activity along the LFZ not only during the Middle Miocene, but possibly also during Late Cretaceous-Palaeogene and Late Miocene-Pliocene times, hence providing additional constraints for the evolution of the Eastern Alps.

2 Geological setting of the Lavanttal Fault Zone and adjacent units

The NNW-trending LFZ is a part of the Pöls-Lavanttal fault system (Frisch et al. 2000; Reinecker 2000), and separates the Koralm Complex in the east from the Saualm Complex in the west (Fig. 2). Both complexes form part of the Central Austroalpine nappe complex. Some models at the scale of the Eastern Alps include the LFZ in general reconstructions of the evolution of faulting during Palaeogene and Neogene times (Neubauer and Genser 1990; Decker and Peresson 1996; Peresson and Decker 1997; Frisch et al. 1998, 2000; Neubauer et al. 2000; Kurz et al. 2001), but little is known about its detailed evolution. These reconstructions, however, show that there is a clear relationship between the Lavanttal fault system and the uplift of Koralm Complex (Neubauer and Genser 1990).

The Pöls-Lavanttal fault system consists of distinct segments showing a right-handed overstep geometry. Dextral offset of approximately 10 km was deduced from displaced lithological units. Vertical offset is 4–5 km, with relative upward movement of the Koralm Complex to the east (Frisch et al. 2000; Reinecker 2000). Near its southern termination, the LFZ cuts and offsets the Periadriatic fault by about 15 km (Figs. 1, 2). The Pöls-Lavanttal fault system is accompanied by intramontane molasse basins (from north to south the Fohnsdorf Basin, Obdach Basin, Lavanttal Basin, see Fig. 2). Particularly the Lavanttal Basin has been interpreted as an oblique graben that formed within a transtensional regime (Frisch et al. 2000) or as an asymmetric, eastward deepening basin (Reischenbacher and Sachsenhofer 2008). Based on the sedimentary evolution of the Lavanttal Basin the LFZ is assumed to be active since Early Miocene times with peaks in activity at 18–16 and 14–12 Ma (Reinecker 2000). At the eastern margin of the Lavanttal Basin, upper Middle Miocene clastic sediments (ca. 12.5–11.5 Ma) are vertically offset. Successive syntectonic sediments indicate a period of continued fault activity between ca. 11 and 5.5 Ma (Reischenbacher and Sachsenhofer 2008). Fault plane solutions for recent seismicity display clear dextral strike-slip movements (Reinecker and Lenhardt 1999; Reinecker 2000). Although displacement is predominantly accommodated along the main fault zone at the western margin of the Koralm Complex, which is several hundred meters wide, distinct sets of subparallel shear zones and faults can be observed towards the central parts of the Koralm massif as well.

According to Hejl (1997, 1998), the units adjacent to the LFZ were already exhumed to a depth of approximately 5–8 km at the beginning of the Cenozoic (from approx. 60 Ma onwards). As indicated by zircon fission track (ZFT) ages, the northern part of the Koralm Complex cooled to temperatures below 200°C already during Late Cretaceous times (Hejl 1997, 1998). In the Pohorje region farther southeast (Figs. 1, 2), ZFT ages indicate Late Oligocene to Middle Miocene cooling of metamorphic rocks (26–15 Ma, Fodor et al. 2003, 2008).

Apatite fission track (AFT) ages from the Koralm Complex become gradually younger from north to south (Hejl 1998). This indicates that the southern parts were cooled later through the apatite partial retention zone. In the central part of the Koralm Complex, AFT ages range from 50 to 37 Ma (Hejl 1998; Rabitsch et al. 2007), whereas ages from 31 to 26 Ma were reported from the southern and western margin of the Koralm Complex (Hejl 1998). Two AFT ages located close to the LFZ show cooling below ~120°C between 28.5 and 18 Ma, and along the western boundary of the LFZ, AFT ages range from ~27 to 12 Ma (Puch 1995).

The subsidence of the Styrian Basin adjacent to the Koralm Complex started around 18 Ma (Ottnangian stage of the Central Paratethys palaeogeographic realm; see Piller et al. 2004). In the southern part of the western Styrian Basin, close to the Pohorje Mountains (Figs. 1, 2), early Miocene sediments lacking a thermal overprint contain apatite grains with a cooling age of ~19 Ma (Eggenburgian). This is only 1–2 Ma older than the time of deposition (Sachsenhofer et al. 1998). As these are detrital ages, they must reflect the timing of exhumation of the source. The cooling rate of the mainly Austroalpine source

was very fast, pointing to tectonic denudation and/or a high geothermal gradient (Sachsenhofer et al. 1998). In the Lavanttal Basin, a phase of coarse-grained clastic input from the east (i.e., from the Koralm massif) is documented for the Sarmatian stage of the Central Paratethys palaeogeographic realm (~12 Ma, Reischenbacher et al. 2007). From the Late Pannonian (~7 Ma) onwards, the terrestrial sedimentary influence increased due to continuing uplift of the Koralm Massif (Ebner and Sachsenhofer 1995; Sachsenhofer et al. 1997, 2001).

3 Internal structure of the Lavanttal Fault Zone

Surface exposures of fault rocks related to the LFZ are rather scarce and are usually strongly weathered. We therefore took samples from three drill cores penetrating segments of the LFZ (drilling sites are shown in Fig. 2). These drill cores were taken as part of the geological and geotechnical site investigations for the Koralm railway tunnel (to be built under the Koralm Massif with a length of 32.8 km) (Fig. 2) (Harer and Otto 2000; Vavrovsky et al. 2001; Steidl et al. 2001). Reconstructions of the LFZ structure from pilot tunnel excavations (Pischinger, Otto, communications) show that the LFZ is characterized by zones of fractured and disintegrated host rock (HR) material (paragneisses alternating with pegmatite gneisses), and domains of cataclastic fault rocks with thicknesses between a few centimetres and several meters. Following the fault zone classifications of Chester et al. (1993), Caine et al. (1996), Faulkner et al., (2003, 2010), and Brosch and Kurz (2008) this internal structure can be described in terms of a succession of HRs, a damage zone (DZ) and a fault core at a scale of a few decimetres to meters (Fig. 3). These domains recur several times along the investigated drill core sections. From this it can be assumed that the displacement along the LFZ is internally partitioned into distinct cataclastic shear zones. We are aware, however, that the sampled drill cores only intersect a small part of the entire fault system.

In the drill core sections, the transition from the HR to the DZ is usually gradual over distances of centimeters to decimeters. The HRs are partly injected by veins indicating hydrothermal fluid activity. Microstructures indicate a strong alteration of the HR close to shear zones (Wölfler et al. 2010). Along the transition to the fault-related rocks the occurrence of secondary shear fractures, irregular veins and fracture networks increases. This transition zone is marked by a few, mm thick, injection veins branching into the HR (Wölfler et al. 2010). The DZ and fault core domains are separated by a sharp boundary marked by shear zones with ultracataclasites (fault rock terminology according to Brodie et al. 2002).

The DZs are characterized by angular HR fragments with a fragment size usually between 0.5 and 5 cm, either clast-supported or partly separated by a fine grained, poorly foliated matrix (Fig. 3). The original HR fabric can still be recognized. Displacement along shear fractures is generally of the order of a few millimetres. Some rock fragments are transected by healed extensional cracks.

Fault core domains are characterized by lens-shaped fragments with a size of 0.5–1 cm in a fine-grained, foliated, dark matrix (Fig. 3). Clay mineral formation by transformation of feldspars is commonly localized along distinct zones of shear localization with a thickness of only a few millimetres (Fig. 3).

4 Sample description

In this study we present data from three drill cores situated at the western margin of the Koralm Massif (Fig. 2). Drill cores KB-D12/02 and KB-D13/03 transect the LFZ, drill core TB-D02/02 is from within the western part of the central Koralm Massif.

$^{40}Ar/^{39}Ar$ dating was carried out exclusively within the LFZ in order to determine the influence of cataclastic deformation and/or hydrothermal fluids on the $^{40}Ar/^{39}Ar$ system in white mica. Fission track and (U/Th)-He-dating have been carried out both within the LFZ (KB-D12/02) and in the central western Koralm Massif (TB-D02/02) to analyze potential differences between ages from the margin and the internal parts of the Koralm massif, i.e. along and away from the LFZ. AFT and (U/Th)-He-ages from these two cores were already described in detail by Wölfler et al. (2010). As KB-D12/02 and KB-D13/03 are located quite close to each other, only the better preserved drilling KB-D12/02 was used for fission track dating. For this purpose, samples were taken as coupled DZ and adjacent HR pairs, and/or as pairs of fault core (FC) cataclasites and the adjacent DZ. This allows to obtain faulting-related resetting of various thermochronological systems within the distinct domains of the LFZ. For $^{40}Ar/^{39}Ar$ dating, samples were taken from the protolith and the adjacent DZ and/or fault core cataclasites. The labelling of samples displayed in Fig. 4, and used in later figures and in the data tables, is related to drilling depth.

Drill core TB-D02/02 cuts a fault segment in the western central part of the Koralm complex (Pischinger et al. 2008). This fault segment, not exposed at the surface, strikes approximately northward, i.e. subparallel to the Lavanttal fault system, and dips steeply toward east. The cataclastic shear zone penetrates a coarse-grained pegmatite gneiss. A clearly developed north-trending shear zone boundary discordantly cutting the pegmatite gneiss foliation dips steeply toward east. The samples from this drill core

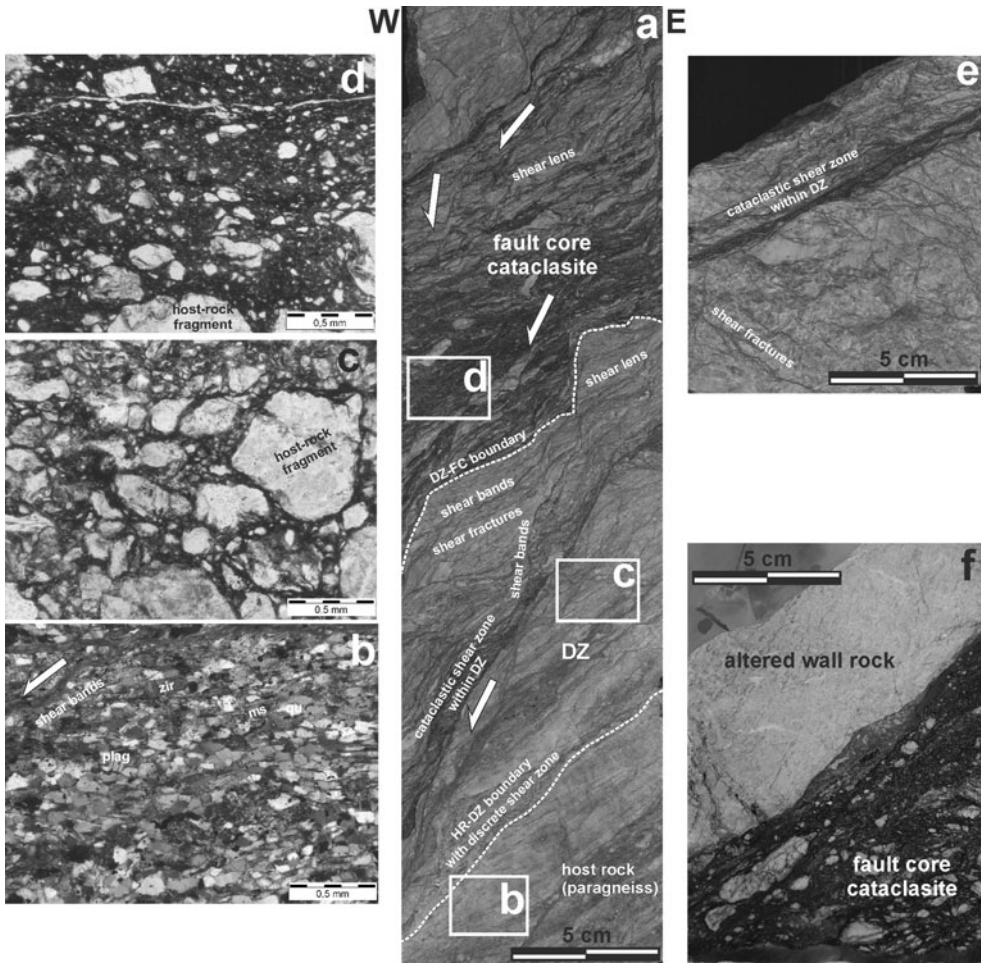

Fig. 3 Meso- and microscale fabrics representative for the internal structure of the LFZ from drilling KB-D13/02 (depth 61.3–66 m). **a** Polished drill core section (KB-D13/02, depth 61.3–61.7 m), with the transition from a paragneiss protolith and an adjacent DZ to a cataclastic fault core. For location of drilling site, see Fig. 2. **b** Protolith microstructure representing the original fabrics, slightly modified by transecting shear bands (KB-D13/02, depth 61.3). *qu* quartz, *plag* plagioclase, *ms* muscovite, *zir* zircon. **c** Microstructure from the DZ–fault core transition, showing HR fragments bordered by shear fractures and partly surrounded by fine-grained fault gouge (*dark*) (KB-D13/02, depth 61.5). **d** Microstructure from the fault core, showing a matrix-supported cataclasite. The matrix (*dark*) mainly consists of clay minerals and ultrafine-grained quartz, the embedded fragments are derived from the protolith (KB-D13/02, depth 61.6). **e** Close-up view of the DZ–fault core transition, showing the development of shear fractures and cataclastic shear zones (KB-D13/02, depth 61.45). **f** Polished drill core section from drilling KB-D13/02 (depth 66 m) with a cataclastic shear zone bordered by strongly altered, bleached HR mainly consisting of albite (from Wölfler et al. 2010, modified). Photos **b**–**d** were taken with crossed polarizing filters

comprise two fine grained cataclasites (samples 425FC, 458FC), one strongly fractured paragneiss (sample 458DZ), and an unfractured micaceous gneiss (sample 426HR).

Drill core KB-D12/02 cuts the main subvertical fault segment along the western margin of the Koralm massif at an angle of 45° and transects a number of sub-parallel segments of the LFZ, consisting of recurring HR, DZ and fault core domains. After a 7 m thick succession of Quaternary deposits, this drill core is characterised by a fault zone divided into a 20 m broad fault core with fault gouges (sample 28FC) and a 29 m wide DZ (samples 28DZ, 56DZ). Between 56.8 and 58 m depth an unfractured HR is represented by coarse grained pegmatite (sample 56HR). The other sample pair from this drill core covers the transition from a DZ (sample 107DZ) to the HR (sample 106HR) consisting of a foliated hydrothermally altered gneiss body.

Drill core KB-D13/02 is close to KB-D12/02 and cuts the western boundary of the Koralm massif and the transition to the LFZ. The samples from this drill core were used especially for $^{40}Ar/^{39}Ar$ dating of white mica, as the drill core transects a wide variety of mica-bearing protoliths (paragneisses, eclogite-amphibolites and pegmatite gneisses,

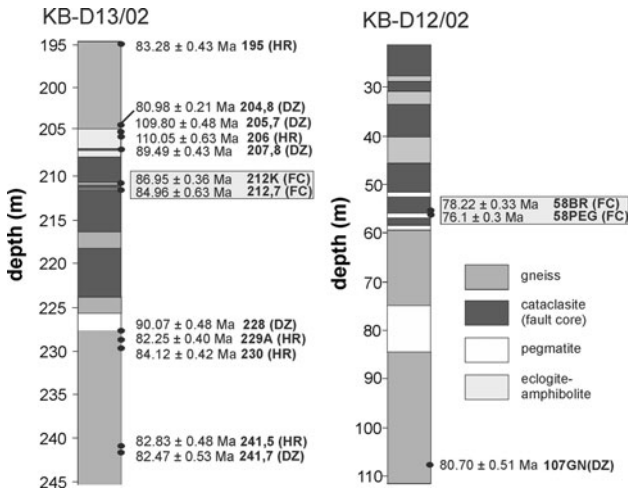

Fig. 4 Schematic lithologs of parts of drill cores KB-D13/02 and KB-D12/02, with the sampling sites for $^{40}Ar/^{39}Ar$ dating of muscovite and the corresponding integrated plateau ages. For location of sampled drilling sites, see Fig. 2. Samples from fault cores are highlighted. *FC* fault core, *DZ* damage zone, *HR* host rock

Fig. 4), all of them affected by cataclastic faulting. Muscovites were separated either from paragneiss protoliths, mainly consisting of plagioclase, quartz, muscovite, and minor amounts of hornblende, or from distinct shear zones and shear planes. Samples KB-D13/02-205.7 and KB-D13/02-206 (Figs. 4, 5) were taken from garnet amphibolites interpreted to be derived from eclogites (so-called eclogite-amphibolites). KB-D13/02-212K, KB-D13/02-212.7, KB-D12/02-58BR, and KB-D12/02-58PEG (Figs. 4, 5) were taken from pegmatite gneisses, also affected by cataclastic shearing. In these cataclastic shear zones muscovite was incorporated within fault rocks and distinct shears subparallel to the shear zone boundaries. Along single shear fractures, muscovite was smeared out along the shear planes. From these, the muscovites were removed directly by hand picking. The sampling positions along the drill cores are displayed in Fig. 4, and the $^{40}Ar/^{39}Ar$ dating results are represented in Fig. 5. The detailed analytical results are published as electronic supplementary material on the journal website (Electronic Supplementary Material, Online Resource 1).

5 Methods used for thermochronology

Tectonic reconstructions in the brittle field are an exercise fraught with uncertainties, and their reliability is strongly dependent on accuracy of deformation dating. Different approaches have been applied, such as (a) direct dating of syntectonic minerals grown on fault planes (e.g. Freeman et al. 1997; Zwingmann and Mancktelow 2004); (b) reconstruction of exhumation histories in distinct fault-bounded blocks (e.g. Bigot-Cormier et al. 2006; Malusá et al. 2005, 2006; Wölfler et al. 2008); (c) correlation among fault-rock types, deformation mechanisms, hydrothermal regimes and low-temperature geochronometers (Malusá et al. 2009); (d) thermochronological analyses of low-temperature systems at short distance across fault zones (Murakami et al. 2002; Tagami and Murakami 2007); (e) combination of some of these approaches (Siebel et al. 2010). In this work, we will follow the approach that near-surface brittle faulting may lead to thermal anomalies by infiltration of hydrothermal fluids or frictional heating (e.g., Maddock 1983; d'Alessio et al. 2003; Otsuki et al. 2003; Wölfler et al. 2010). As deformation along the LFZ is heterogeneously distributed and is typically concentrated along distinct cataclastic shear zones that accommodate displacement of relatively rigid wall rocks, the effect of frictional heating should be extremely localized and restricted to zones of a few centimetres thickness adjacent to the fault surface. Murakami et al. (2006) estimated that for a temperature range of 400–1,000°C along a fault plane ZFTs will only be affected within a distance of 2.5 mm and therefore concluded that the main mechanism of heat transfer in fault zones is fluid-related. In contrast to shear heating, hydrothermal fluids penetrating a fault zone may affect a wider area and leave a mark of thermal influence within the DZ and adjacent HR. Along the LFZ, hydrothermal activity is indicated by the precipitation of quartz and ore minerals within extensional cracks and tension gashes, and by the alteration of the wall rocks along distinct shear fractures and shear zones (Wölfler et al. 2010) (Fig. 3).

We have chosen thermochronological systems characterized by closure temperatures between ~400°C and approximately ~40°C. New data from $^{40}Ar/^{39}Ar$ dating on white mica and ZFT dating are combined with recently published AFT and apatite (U-Th)/He ages (Wölfler et al. 2010) from the same fault zone. For the thermochronological systems applied in this study, annealing and retention depend not only on heating temperature, but on heating duration as well (Laslett et al. 1987; Murakami et al. 2006). Thermochronometry should provide information on the timing of thermal events related to shearing along the LFZ and on the exhumation of the fault zone and adjacent units. The following thermochronological methods were used.

5.1 $^{40}Ar/^{39}Ar$ dating

The $^{40}Ar/^{39}Ar$ analytical techniques follow those described by Handler et al. (2004). The preparation of the samples before and after irradiation, the $^{40}Ar/^{39}Ar$ analyses, and the age calculations were carried out at the ARGONAUT Laboratory of the Department of Geography and Geology

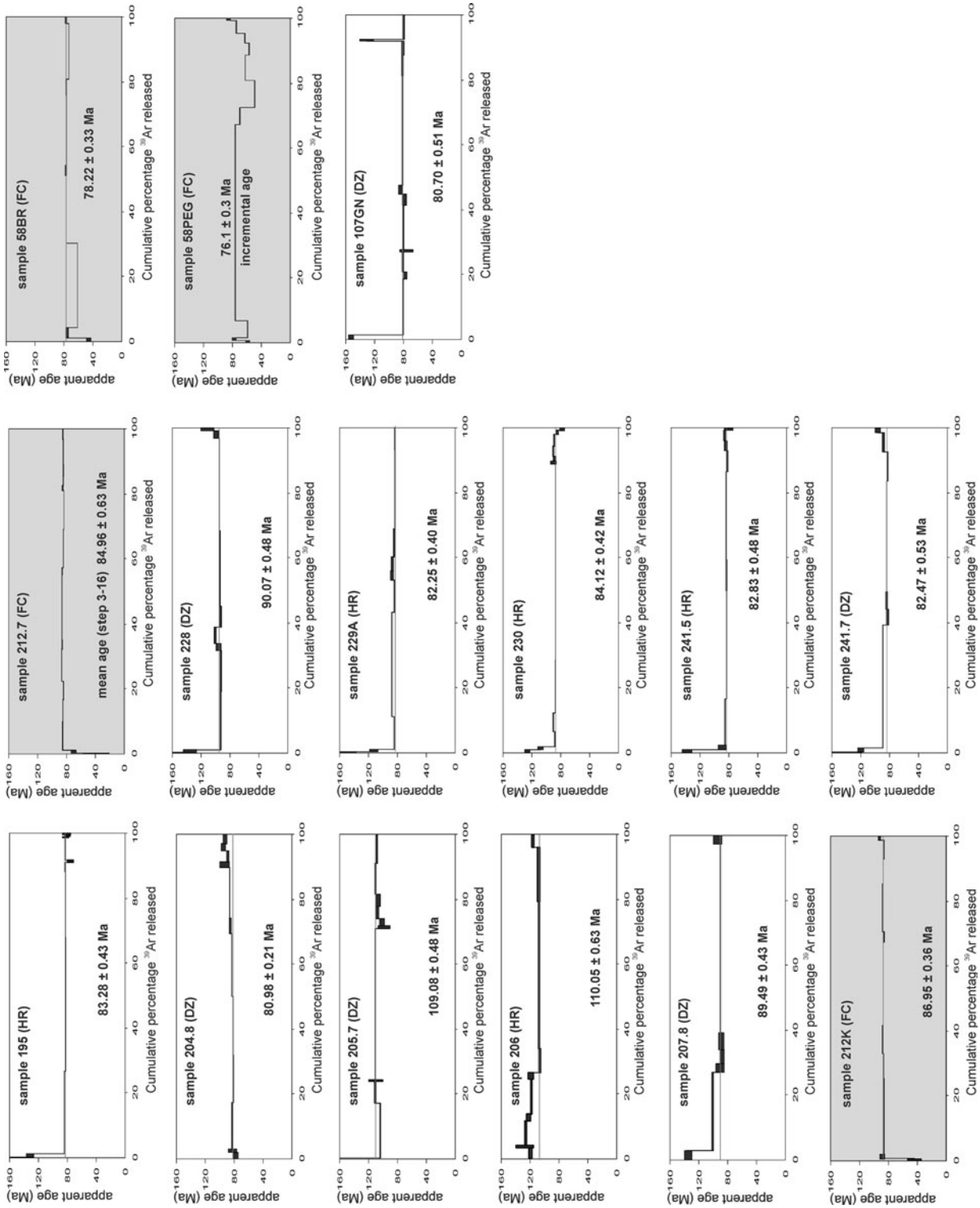

Fig. 5 $^{40}Ar/^{39}Ar$ apparent age spectra. For location of sampling sites see Fig. 4. Laser energy increases from left to right until fusion. Width of the bars represents 2σ error. Release spectra from cataclastic shear zones are highlighted. *FC* fault core, *DZ* damage zone, *HR* host rock. For location of sampled drilling sites, see Fig. 2

at the University Salzburg. For additional details about the sample preparation and irradiation procedures, see Wiesinger et al. (2006).

The samples are characterized by the accumulation of white mica along shear fractures within the DZ domains, and along cataclastic shear zones within the fault core domains. Mineral concentrates were prepared by crushing, sieving, flotation, and hand-picking of the grain-size 200–250 μm. For measurements, 10–15 grains were finally used. In addition to muscovite multigrain samples, single grains from cataclastic shear zones were analyzed in order to reveal the influence of deformation on Ar diffusion and/or resetting in the crystal lattice.

The closure temperature of the Ar isotopic system in white mica has been reported to be relatively low, and ranges from ca. 350°C (Lips et al. 1998) to ca. 450°C (Hames and Browning 1994; Kirschner et al. 1996) and ca. 500°C (Hammerschmidt and Frank 1991; Hames and Cheney 1997). Closure temperatures depend on grain-size, chemical composition and cooling rate. Moreover, several studies (e.g., Chopin and Maluski 1980; von Blanckenburg and Villa 1988; von Blanckenburg et al. 1989; Dunlap 1997; Bossé et al. 2005) have revealed that temperature is not the only controlling factor for setting or re-setting the isotopic system within minerals (see also Villa 1998, for a general discussion) and deformation can be of equal importance (e.g., Chopin and Maluski 1980; Müller et al. 1999; Kurz et al. 2008).

5.2 Fission track and (U-Th)/He dating

We used ZFT, AFT, and apatite (U-Th)/He dating methods with partial retention or annealing zones (ZPAZ, APAZ, HePRZ), between 300 and 200, 120 and 60, 85 and 40°C, respectively (Wagner and Van den haute 1992; Green et al. 1986 for APAZ; Tagami and Shimada 1996 for ZPAZ, Wolf et al. 1998 for HePRZ).

Fission track and (U-Th)/He analyses were carried out in the Thermochronological Laboratory of the University of Tübingen (Germany) using standard procedures described by Farley (2002) and Wölfler et al. (2008). The AFT and (U-Th)/He analytical procedures are described in detail by Wölfler et al. (2010), as well as the procedures of thermal history modelling. The zircon mounts were etched in a KOH–NaOH eutectic melt at 215°C (Gleadow et al. 1976; Zaun and Wagner 1985) for 30 h. Track lengths were measured on horizontal confined tracks, revealed as tracks-in-tracks. We followed the methods described by Tagami and Murakami (2007). We therefore adopted tracks with orientations >60° to the crystallographic c-axis because of enhanced anisotropy in annealing and etching for tracks <60° (Hasabe et al. 1994). The zeta calibration approach (Hurford and Green 1983) was adopted to determine the ages. FT ages were calculated with the program TRACKKEY version 4.1 (Dunkl 2002). Modelling of the low temperature thermal history was carried out using the HeFty modelling program by Ketcham (2005), with Dpar values (mean diameters of the etch figures on prismatic surfaces of apatites parallel to the crystallographic c-axis, see Burtner et al. 1994) as kinematic parameter.

The annealing behavior of fission tracks in zircon samples is highly sensitive to α-damage, in particular in the very low α-damage density range (Rahn et al. 2004). Temperatures for total resetting of the FT system depend not only on the annealing duration, but also on the amount of accumulated α-damage. Closure temperatures for the ZFT system may therefore vary over more than 100°C as a function of α-damage (Brandon et al. 1998; Rahn et al. 2004). There is no fixed closure temperature for the ZFT system but the range of the ZPAZ is dependent not only on the cooling rate but also on the U and Th content.

6 Results from geochronology

6.1 $^{40}Ar/^{39}Ar$ dating results

In general, all Ar release spectra from HR and DZ samples (Figs. 4, 5) are characterized by elevated ages for the first heating steps, suggesting the incorporation of extraneous Ar both for protolith- and DZ-derived muscovites. Except for these first heating steps, the Ar release spectra show well-defined integrated plateau ages between ~81 and 90 Ma. Samples from eclogite-amphibolites show older ages around 110 Ma (samples KB-D13/02-205.7 and KB-D13/02-206). These ages were only observed within coarse-grained eclogite-amphibolites, associated with pegmatite. KB-D13/02-204.8 displays a well defined plateau age of ca. 81 Ma.

Fault core samples from cataclastic shear zones (KB-D13/02-212K, KB-D13/02-212.7, KB-D12/02-58BR, KB-D12/02-58PEG), by contrast, show reduced ages for the first experiment increments (Fig. 5). These highly reduced incremental ages are far below the protolith cooling ages described above. Particularly KB-D12/02-58BR shows an incremental age of ca. 43 Ma for the first heating step, significantly lower than the mean ages of the subsequent steps. KB-D12/02-58BR and KB-D12/02-58PEG were sampled from a cataclastic shear zone containing fragments of pegmatite. KB-D12/02-58BR comprises fine-grained pegmatite kakirites consisting of altered pegmatite fragments. The average fragment size is approximately 1 mm. The related muscovite grains are distorted and broken and are smeared out along shear planes. KB-D12/02-58PEG adjacent to the kakirite shear zone of KB-D12/02-58BR comprises pegmatite fragments with a size between 0.5 and

5 cm and remnants of coarse grained distorted muscovite grains. KB-D13/02-212K comprises fine-grained kakirites consisting of strongly altered pegmatite gneiss fragments with an average size of approximately 1 mm.

The integrated plateau ages of 85–87 Ma (KB-D13/02-212K, KB-D13/02-212.7) for the subsequent heating steps are similar to the protolith plateau ages described above. Only KB-D12/02-58BR and KB-D12/02-58PEG, derived from a cataclastic shear zone, show integrated plateau ages and incremental ages being more than 2 Ma younger (76–78 Ma). These age spectra therefore indicate Ar loss along the grain boundaries assuming that during stepwise heating Ar will be released from the muscovite rims at first.

6.2 Zircon fission track dating results

In both analyzed drill cores (KB-D12/02, TB-D02/02), ZFT central ages range between 77.6 ± 5.5 and 64.8 ± 4.6 Ma both within fault and HRs (Fig. 6; Table 1). Although all four fault/HR sample-pair central ages overlap within the 1σ error, there is a trend of decreasing ages towards the fault rocks, particularly for samples 28FC (68.3 ± 5.0 Ma) and 458FC (70.3 ± 5.0 Ma). Track lengths were additionally analyzed and demonstrate reduced mean track lengths (MTL) of 7.13 ± 1.56 and 8.22 ± 1.67 µm in fault core samples 28FC and 458FC, respectively. By contrast, the samples from HRs and DZs show MTLs in the range of 10.00 ± 0.97–10.42 ± 1.03 µm (Fig. 6; Table 1). Particularly within the DZs and fault cores, but also in HRs close to fault zones, single grain ages are highly variable and range between ~36.6 and 155 Ma (Fig. 6; Table 2).

6.3 Apatite fission track and (U-Th)/He dating results

The AFT and (U-Th)/He dating results are described in detail by Wölfler et al. (2010) and are therefore just summarized here. Representative results are displayed in Figs. 7 and 8, and an overview of ZFT, AFT and (U-Th)/He ages is provided in Fig. 8.

AFT HR ages not affected by cataclastic deformation range between 51.1 ± 2.3 in the central part of the Koralm massif and 37.7 ± 4.3 Ma along its western margin. Ages from fault-related rocks vary between 46.6 ± 4.7 and 43.3 ± 4.2 in the central part and 43.6 ± 2.1 and 34.3 ± 1.8 Ma along the western margin of the Koralm massif. Single grain ages, however, are variable within all three fault core rocks and range from 76.5 ± 12.3 to 3.6 ± 1.3 Ma. These samples do not pass the chi-square test and can be decomposed into two age clusters related to the skewed age-track length distribution, reflecting some level of annealing (Fig. 7). The two dominant age components yield a weighted mean of 56.1 ± 4.3 and 8.6 ± 2.6 Ma. Furthermore, the samples from the fault cores show significantly reduced MTL (Fig. 7). Dpar measurements from fault core samples indicate a clear relationship between single grain ages, MTL and Dpar values (Wölfler et al. 2010) (Fig. 7). The lowest Dpar values are associated with the youngest single grain ages and the shortest MTL's.

In the (U-Th)/He analyses a clear trend of decreasing ages from the HR toward the DZs and fault cores can be observed (Wölfler et al. 2010) (Fig. 8). The weighted mean age from the HR is 11.8 ± 0.8, from the DZs 7.4 ± 0.4 and 6.2 ± 0.4 Ma, and 4.7 ± 0.3, 5.7 ± 0.5 and 4.8 ± 0.3 Ma from the fault cores.

It is generally assumed that both high chlorine-content in apatites and large Dpar values indicate enhanced resistance against annealing (e.g., Green et al. 1986; Carlson et al. 1999; Barbarand et al. 2003). Recent studies have demonstrated, however, that Dpar values need not necessarily correlate with chlorine but may correspond with the Si content (Spiegel et al. 2007), or reflect the complex interactions between anion (Cl, F, OH) and cation (REE, Mn, Sr) substitutions (Barbarand et al. 2003). However, the single grain-age–Dpar and MTL–Dpar relationships as shown in Fig. 7 indicate that secondary heating is reflected by different annealing behaviour due to different kinetic properties of the apatites. Even though we cannot exclude that apatites from HR-derived fragments, embedded within a fault gouge matrix, contribute to the older AFT age groups within the fault core samples, at least partial annealing in cataclastic shear zones is beyond doubt.

6.4 Results from thermochronological modelling

Thermal history modelling for two HR samples suggests cooling to the level of the lower APAZ boundary in the Eocene, followed by thermal stagnation at these temperatures and accelerated final cooling during Late Miocene times (Fig. 9). Zircon/apatite pairs from HR samples indicate slow cooling on the order of 4.3°C Ma^{-1} for the samples from drill core KB-D12/02 (sample 106HR) and 5.1°C Ma^{-1} for those from drill core TB-D02/02 (sample 426 HR) between Late Cretaceous and Palaeocene to Eocene times.

7 Implications for the evolution of the Lavanttal Fault Zone and adjacent units

The comparison of thermochronological age data from distinct structural domains provides new information on the evolution of the LFZ and the adjacent Koralm Massif. Several thermochronological systems indicate at least partial thermally and/or mechanically induced deviation

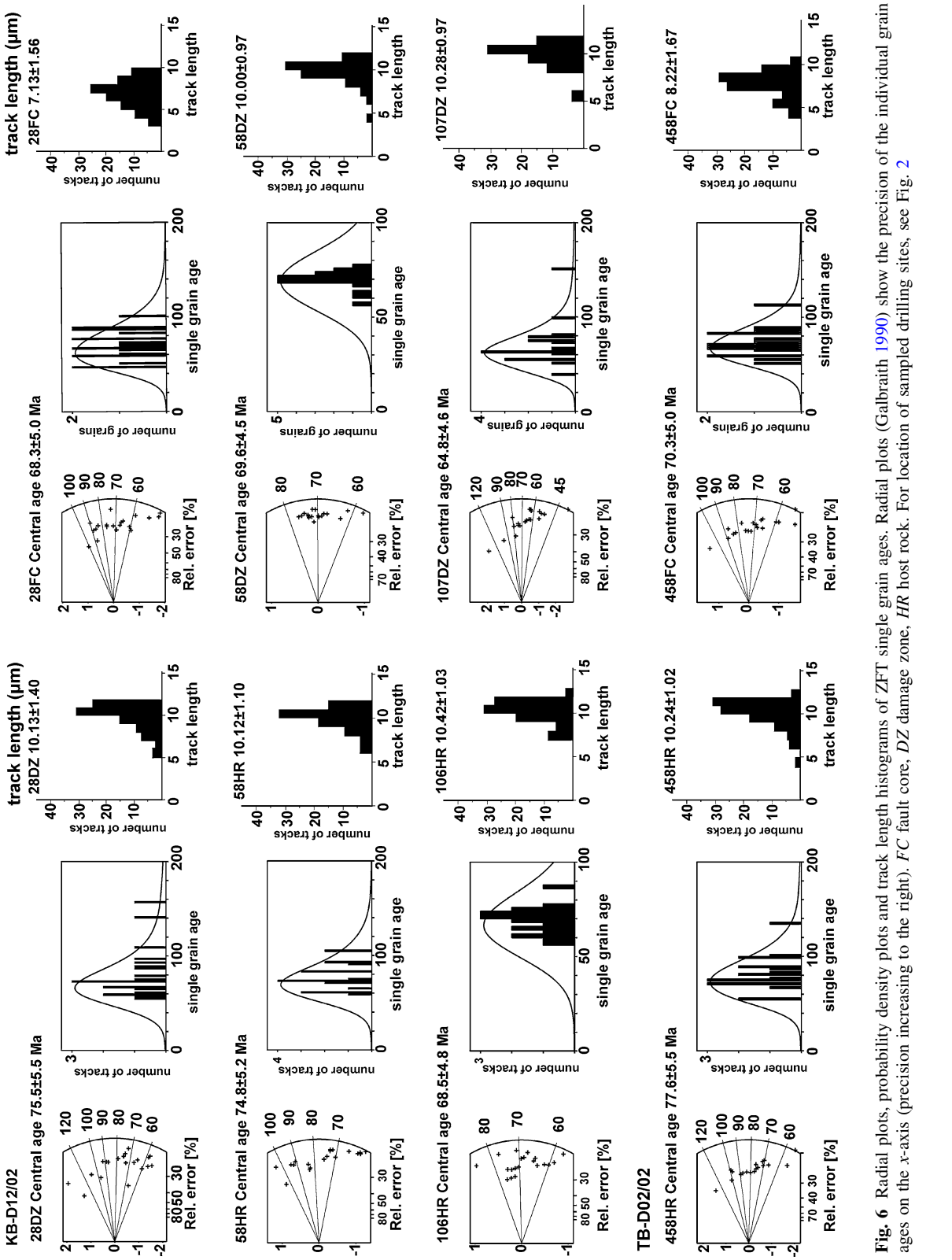

Fig. 6 Radial plots, probability density plots and track length histograms of ZFT single grain ages. Radial plots (Galbraith 1990) show the precision of the individual grain ages on the *x*-axis (precision increasing to the right). *FC* fault core, *DZ* damage zone, *HR* host rock. For location of sampled drilling sites, see Fig. 2

Table 1 Analytical results of ZFT dating

Sample code	Drill core	Depth (m)	N	ρ_s	N_s	ρ_i	N_i	ρ_d	N_d	$P(\chi^2)$ (%)	Age (Ma)	$\pm1\sigma$ (Ma)	MTL (μm)	SD (μm)	N(l)
28FC	KB-D12/02	28.2	20	4.602	873	2.583	490	6.345	12,047	80.62	68.3	5.0	7.13	1.56	52
28DZ	KB-D12/03	28.8	20	4.855	902	2.541	472	6.543	12,047	53.23	75.5	5.5	10.13	1.40	70
58DZ	KB-D12/04	58.2	20	6.597	1,297	3.616	711	6.322	12,047	100.00	69.6	4.5	10.00	0.97	70
58HR	KB-D12/05	58.8	20	5.682	1,117	4.592	552	6.121	12,047	95.70	74.8	5.2	10.12	1.10	72
106HR	KB-D12/06	106.2	20	5.035	970	2.875	554	6.477	12,047	99.99	68.5	4.8	10.42	1.03	70
107DZ	KB-D12/07	107.3	20	4.744	900	2.783	528	6.291	12,047	55.48	64.8	4.6	10.28	0.97	72
458FC	TB-D02/02	458.0	20	5.840	953	3.340	545	6.655	12,047	94.84	70.3	5.0	8.22	1.67	74
458HR	TB-D02/03	458.8	20	6.104	996	3.150	514	6.633	12,047	85.04	77.6	5.5	10.24	1.02	74

N is number of dated zircon crystals; ρ_s/ρ_i spontaneous/induced track densities ($\times10^5$ tracks/cm^2); N_s/N_i is number of counted spontaneous/induced tracks; ρ_d dosimeter track density ($\times10^5$ tracks/cm^2); N_d number of tracks counted on dosimeter; $P(\chi^2)$ probability obtaining chi-square value (χ^2) for n degree of freedom (where n is number of crystals -1); age $\pm$ 1σ is central age $\pm$ 1 standard error; Comp. 1 and 2: different age components in samples; *MTL* mean track length; *SD* standard deviation of track length distribution; N (l) number of horizontal confined tracks

Table 2 Analytical results of ZFT dating—single grain ages

28FC		28DZ		58DZ		58HR		106HR		107DZ		458FC		458HR	
Age (Ma)	$\pm1\sigma$ (Ma)	Age (Ma)	$\pm1\sigma$ (Ma)	Age (Ma)	$\pm1\sigma$ (Ma)	Age (Ma)	$\pm1\sigma$ (Ma)	Age (Ma)	$\pm1\sigma$ (Ma)	Age (Ma)	$\pm1\sigma$ (Ma)	Age (Ma)	$\pm1\sigma$ (Ma)	Age (Ma)	$\pm1\sigma$ (Ma)
47.6	7.9	57.2	14.8	57.1	11.6	59.6	12.4	58.4	13.7	39.6	7.8	52.7	12.3	56.5	11.0
47.9	10.6	59.4	15.5	62.7	12.5	60.4	13.1	58.8	12.6	53.3	12.3	54.6	10.6	56.7	13.2
51.8	12.1	60.6	14.0	64.2	14.0	62.1	13.6	59.0	14.0	55.7	12.7	58.4	13.1	66.5	15.3
59.0	13.4	61.3	14.3	66.7	13.7	62.9	13.9	59.5	16.1	56.6	13.7	59.6	13.4	70.0	16.2
59.5	16.3	62.8	16.9	67.4	14.0	70.2	14.6	59.7	14.4	57.5	12.8	65.0	15.8	70.3	15.2
61.0	15.9	67.8	16.3	67.4	14.0	71.5	16.5	61.1	14.7	62.5	13.5	66.9	14.7	71.1	15.6
65.6	15.9	69.8	17.3	68.2	14.3	73.2	15.5	64.9	14.9	63.7	15.6	68.1	14.9	73.5	17.4
66.6	16.5	70.3	17.1	69.0	14.7	74.2	15.9	66.6	15.0	64.0	14.2	68.9	16.0	75.5	17.2
67.4	17.3	75.4	15.9	69.5	14.3	74.2	15.9	69.1	15.4	65.1	15.9	70.4	17.1	75.8	18.9
69.7	19.0	77.1	17.2	70.1	14.9	75.4	17.2	69.3	14.6	65.1	15.9	70.6	16.0	77.6	18.9
73.6	15.6	78.2	18.0	72.1	14.2	76.8	18.1	69.6	17.2	74.6	19.7	71.1	17.9	78.9	19.9
76.9	19.7	78.9	20.4	72.7	16.5	84.3	22.2	72.0	18.4	76.4	19.6	75.7	19.3	82.3	21.1
78.4	20.0	85.6	20.5	73.0	14.4	84.7	22.8	72.6	16.3	78.1	20.5	77.1	17.5	85.9	21.8
80.4	20.4	90.6	24.5	73.3	15.6	85.1	21.4	73.7	21.7	78.1	20.5	77.4	19.6	85.9	21.8
83.9	21.6	90.9	22.5	73.4	15.7	92.5	22.5	73.7	18.8	80.5	24.6	80.8	20.8	87.9	22.8
86.5	23.3	92.7	22.8	73.5	15.4	94.1	23.8	74.1	21.2	92.6	22.6	80.8	20.8	87.9	22.8
87.9	28.2	98.7	23.7	74.5	15.8	95.8	24.2	75.9	22.2	93.2	26.2	82.6	21.6	96.5	24.1
89.0	24.5	109.8	27.5	74.6	15.6	98.4	32.2	76.9	19.9	93.2	23.2	85.9	21.0	97.6	23.8
90.2	22.5	141.7	35.6	75.7	15.6	98.3	27.9	79.2	17.0	99.7	30.1	86.1	24.3	98.2	27.6
101.2	35.9	157.8	55.3	78.6	16.1	103.1	34.1	87.8	22.2	155.2	61.4	116.7	44.3	137.8	47.4

from the ages in HRs adjacent to the LFZ. As reported by Wölfler et al. (2010) the occurrence of a second, young AFT age population in fault core samples and the decrease of MTL's and apatite (U-Th)/He ages towards the fault cores indicate substantial heat advection into the fault zone. The trend of younger (U-Th)/He ages in the fault cores compared to the DZs is considered to reflect the final evolution of the LFZ. Heat transfer was high enough to partly reset the AFT ages in the fault cores, but not in the DZs (Wölfler et al. 2010). From the degree of resetting of the various thermochronological systems we assume that temperatures within the LFZ were in the range of the ZPAZ–APAZ transition and therefore resetting of both systems remained incomplete.

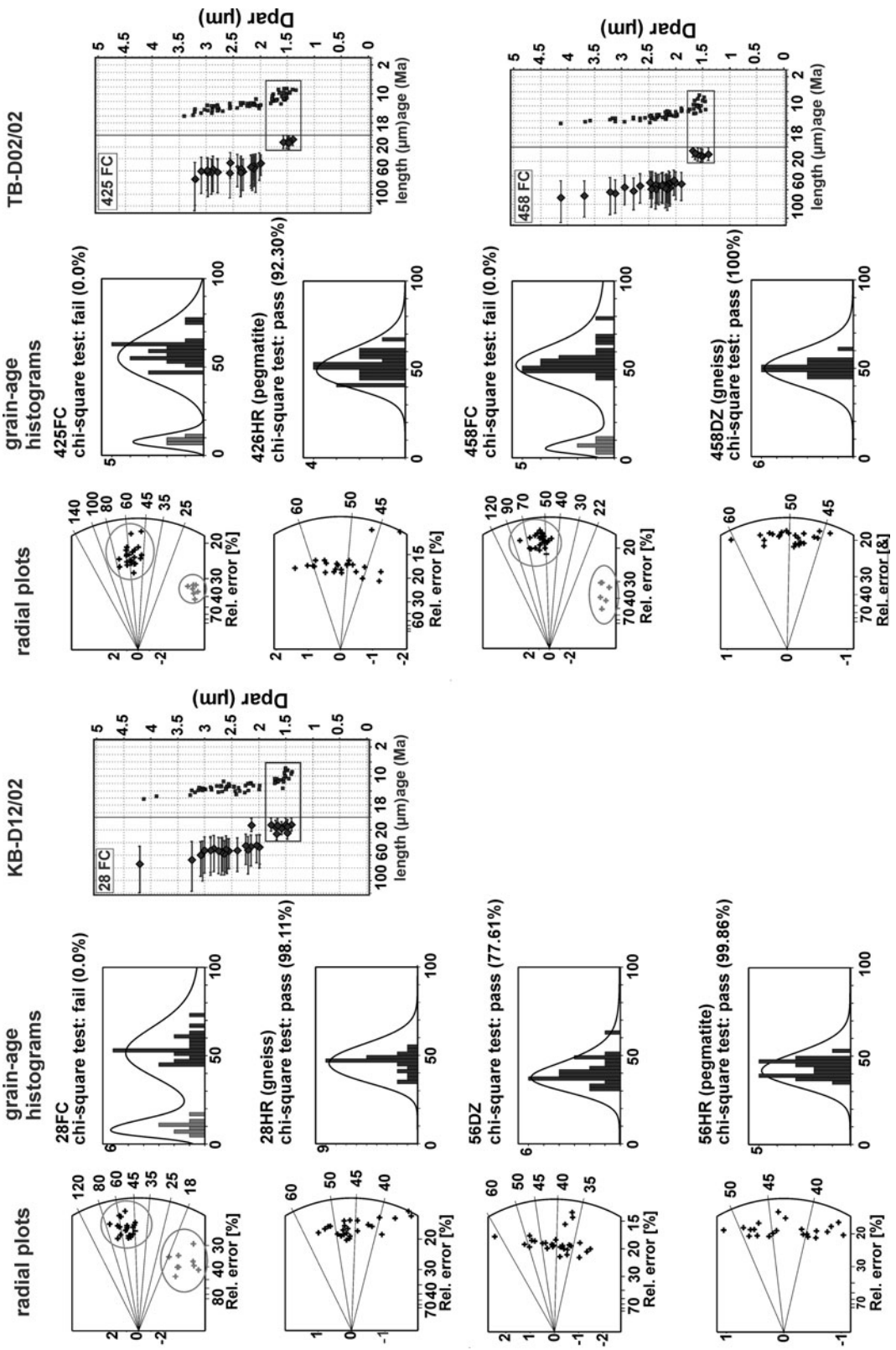

Fig. 7 Radial plots, track length histograms, AFT single grain ages versus track length and Dpar (only for fault rock samples) of AFT single grain ages. Radial plots (Galbraith 1990) show the precision of the individual grain ages along the *x*-axis (precision increasing to the right). All three fault core samples are characterized by two age components (*marked*) where the single grain ages from the younger age components range between 12.8 and 3.6 Ma. *FC* fault core, *DZ* damage zone, *HR* host rock. For location of sampled drilling sites, see Fig. 2. The original data as well as radial plots for FC samples and Dpar were published by Wölfler et al. (2010), track length histograms and radial plots for HR and DZ samples are added here

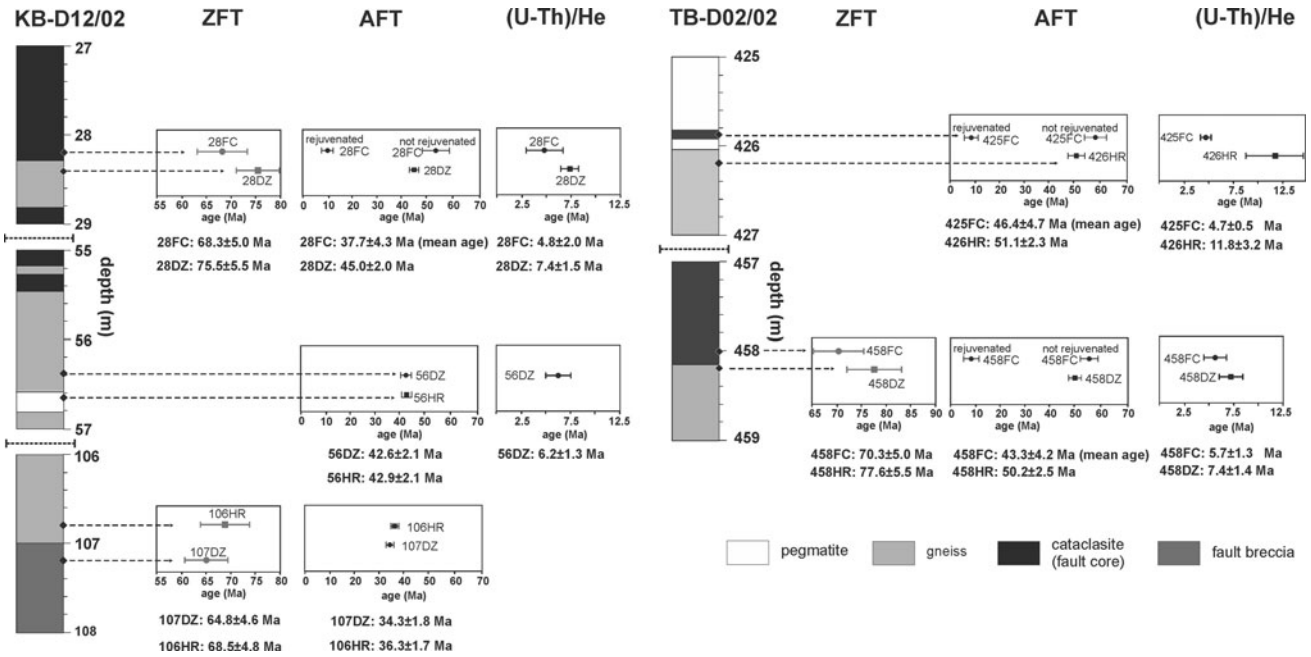

Fig. 8 Compilation diagram comparing the mean age results from ZFT data (this paper) with AFT and (U-Th)/He mean ages (from Wölfler et al. 2010). For location of sampled drilling sites, see Fig. 2. *AFT* apatite fission track ages; *ZFT* zircon fission track ages; *HR* host rock; *DZ* damage zone; *FC* fault core

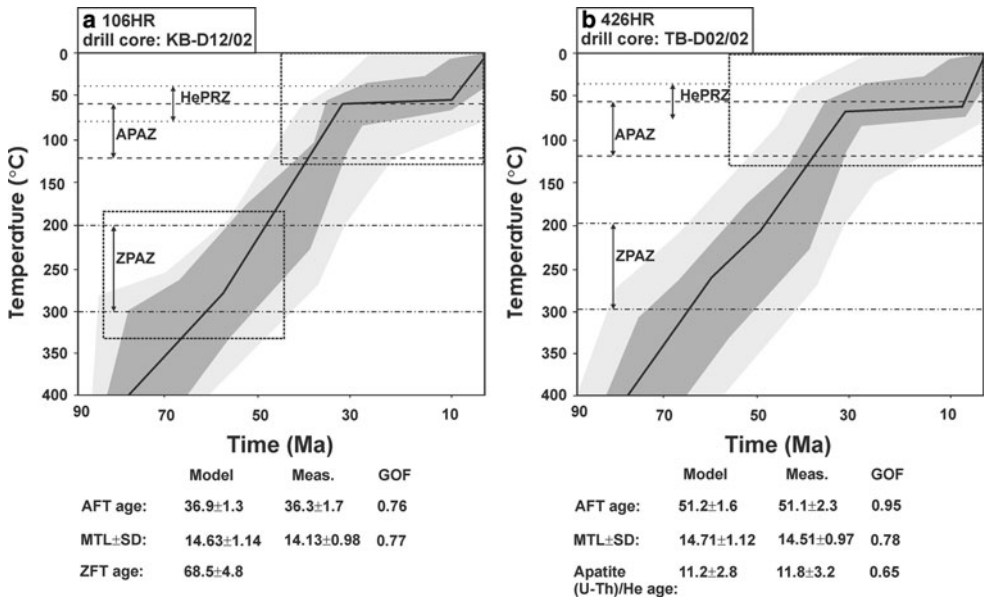

Fig. 9 Results of fission track and (U-Th)/He thermal history modelling using the HeFTy program package (Ketcham 2005). The lower temperature parts of the models are taken from Wölfler et al. (2010). **a** Thermal history model of HR sample (106HR) from drilling KB-D12/02 calculated from AFT and ZFT ages. **b** Thermal history model of HR sample (426HR) from drilling TB-D12/02 calculated from AFT and (U-Th)/He ages. *Light gray paths*: acceptable fit; *dark grey paths*: good fit; *thick black line*: representative best fit line. AFT modelling: input parameters: weighted mean AFT age with 2σ error, track length distribution, Dpar values as kinetic parameters; multi-kinetic annealing model of Ketcham et al. (1999). Additional geological information like ZFT data was converted into time–temperature constraints in form of boxes for the modelling. The end of the time–temperature paths was set at 20°C. (U-Th)/He modelling: input parameters: uncorrected (U-Th)/He age with 1σ error, sphere radius; activation energy 32.9 kcal/mol; calibration after Farley (2002). *MTL* mean track length; *SD* standard deviation in µm; *GOF* goodness of fit (statistical comparison of the measured input data and modelled output data; a "good fit" corresponds to a value 0.5 or higher, the "best fit" corresponds to the value 1; *boxes with dashed lines*: constraints according to the different partial annealing (ZPAZ, APAZ) and retention zones (HePRZ)

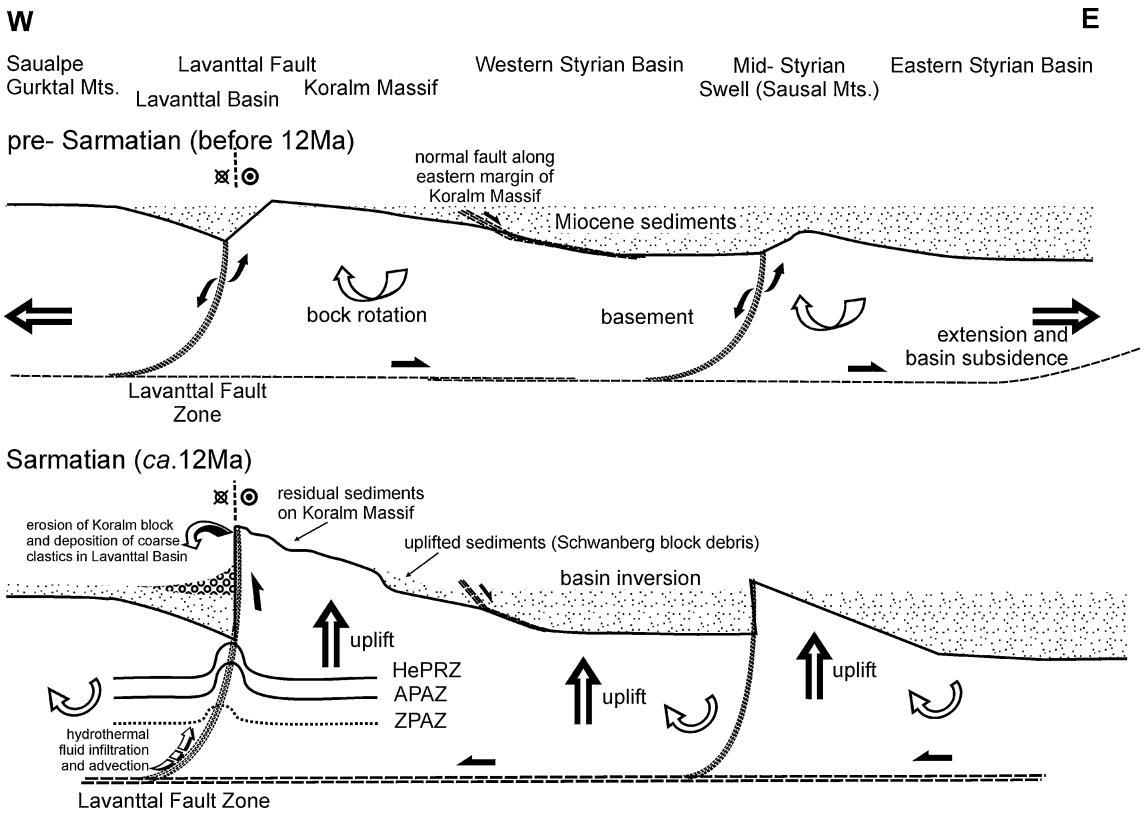

Fig. 10 Schematic cross sections (not to scale) for the evolution of the LFZ and the adjacent Koralm Massif and Styrian Basin during Miocene times. *HePRZ* He partial retention zone; *APAZ* apatite partial annealing zone; *ZPAZ* zircon partial annealing zone

$^{40}Ar/^{39}Ar$ muscovite ages do not provide detailed timing information on fault activity as heat advection into the LFZ was too low to reset the Ar isotopic system completely. ZFT ages were partly reset. The degree of annealing, however, is difficult to estimate.

7.1 Neogene evolution

Beside the constraints on the thermochronological evolution of the LFZ described by Wölfler et al. (2010), the AFT and apatite (U-Th)/He ages provide additional information on the evolution of the adjacent basement blocks and sedimentary basins. The time–temperature history of the Koralm basement indicates thermal stagnation within the upper APAZ to HePRZ during Oligocene to Middle Miocene times (Fig. 9). This time span is the main phase of eastward displacement of Austroalpine units and is surprisingly not displayed by the geochronological data presented in this study. The initial phase of this evolution is, however, mainly characterized by strike-slip displacement along block bounding fault zones (e.g., Ebner and Sachsenhofer 1995; Frisch et al. 2000; Linzer et al. 2002). Particularly in the easternmost part of the Alps this did not result in vertical movements of fault-bounded blocks. The eastern part of the Eastern Alps is characterized by the subsidence of intramontane Molasse basins and of the Styrian basin along the eastern margin of the Koralm massif, starting during Early Miocene times. The Styrian Basin and the Lavanttal Basin were initially limnic-fluvial and subsequently marine (Ebner and Sachsenhofer 1995; Sachsenhofer 1996; Sachsenhofer et al. 1997, 2001; Reischenbacher et al. 2007), indicating a phase of sea-level rise (Piller and Harzhauser 2005). As indicated by remnant clastic deposits on top of the Koralm Massif (Beck-Mannagetta 1980; Nebert 1983) and along the eastern margin of the Saualm Massif and the Gurktal mountains (Dunkl et al. 2005; Reischenbacher et al. 2007, see Fig. 2), the eastern part of the central Eastern Alps was entirely covered by Early Miocene deposits (Fig. 10). A separation into distinct basins started during mid-Miocene times ($\sim$12 Ma), probably related to the differential vertical movement of crustal blocks (Ebner and Sachsenhofer 1995; Pischinger et al. 2008, see Fig. 10). This is reflected by 2 types of age data (cf. Wölfler et al. 2010):

(1) Although the maximum temperature reached in the fault cores cannot be revealed by the AFT data, the timing of fluid flow can be bracketed between the younger AFT group and the (U-Th)/He ages, i.e. in Late Miocene to Early Pliocene times (Wölfler et al. 2010).

(2) The (U-Th)/He age of one HR sample (426HR) shows a weighted mean age of 11.8 ± 0.8 (Fig. 8) (Wölfler et al. 2010). We presume that this age reflects the final cooling of the Koralm basement through the HePRZ. According to the thermal modelling results (Fig. 9), the Koralm Complex was in thermal stagnation between ~30 and 10 Ma, right within the HePRZ, and final cooling started at ~12 to 10 Ma. This was accompanied by vertical displacement along the LFZ, reflected by the annealed AFT age populations (Wölfler et al. 2010) described above. Vertical displacement with relative upward movement of the eastern block is also indicated by shear bands and shear fractures within cataclastic shear zones and the DZ (Fig. 3). This is supported by the vertical offset of clastic sediments of late Mid-Miocene age (ca. 12.5–11.5 Ma) at the eastern margin of the Lavanttal Basin, suggesting a considerable faulting episode during post Mid-Miocene times until ca. 5.5 Ma (Reischenbacher and Sachsenhofer 2008). Subsequent faulting episodes along the LFZ are documented both by partial annealing of AFT single grain ages and resetting of U/Th-He ages within DZs (7.4–6.2 Ma) and fault core cataclasites (5.7–4.7 Ma, see Fig. 8). Previously deposited clastics in the area of the Koralm massif (Fig. 2) were nearly entirely eroded and partly re-deposited in the Lavanttal Basin (Fig. 10). The present elevation of remnant clastic deposits at an altitude of 800–1,100 m indicates that the Koralm massif was uplifted by a minimum of 800 m during post Mid-Miocene times, associated with a phase of E-W-directed extension accommodated by N–S striking normal faults (Pischinger et al. 2008). Although a detailed stratigraphic correlation is missing for these palaeosurfaces, the cooling of the basement below the HePRZ at ~12 to 10 Ma provides an assessment of their minimum age.

Based on these data, together with the sedimentary record from the Lavanttal Basin, it seems likely that the separation of the Lavanttal Basin from the Styrian Basin, now disconnected by the exhuming and uplifting Koralm massif, was related to this tectonic event along the LFZ (Fig. 10). Accordingly, the Lavanttal Basin was initially not formed as a pull-apart basin or oblique graben structure as commonly suggested (e.g., Frisch et al. 2000; Reinecker 2000).

7.2 Age constraints on the pre-Neogene evolution

Up to now the LFZ was assumed to have formed during Early Miocene times within the eastward moving Austroalpine corridor (e.g., Ratschbacher et al. 1991; Frisch et al. 2000; Linzer et al. 2002). The AFT and apatite (U-Th)/He age clearly document that the LFZ formed a thermal anomaly over a period in the range of several million years. $^{40}Ar/^{39}Ar$ muscovite and ZFT ages show that along the LFZ these thermochronological systems were affected as well.

Most $^{40}Ar/^{39}Ar$ muscovite ages provided in this study are in accordance with the ages described from the adjacent Koralm Complex (e.g., Thöni and Miller 1996) and Saualm Complex (Wiesinger et al. 2006). Ages from DZs along the LFZ are similar to ages from HR domains. In other words, the Ar isotopic system was not reset within the DZs. The related plateau ages are therefore interpreted to represent the cooling of the HRs below the closure temperature for the Ar isotopic system in muscovite (approximately 400–450°C, see Chap. 5) during Late Cretaceous times, i.e., between 80 and 90 Ma, subsequent to the peak of metamorphism. Ages of ~110 Ma from eclogite-amphibolites are older than the peak of high-pressure metamorphism within the Koralm Complex (~90 to 100 Ma, cf. Thöni and Miller 1996) and may indicate excess Ar or incomplete rejuvenation during Alpine eclogite and amphibolite facies metamorphism.

Muscovites derived from fault cores of cataclastic shear zones, however, show Ar release spectra characterized by reduced incremental ages for the first steps of heating experiments (Fig. 5). While KB-D13/02-212K and KB-D13/02-212.7 show a common plateau age of ca. 87 and 85 Ma for the subsequent heating steps, KB-D12/02-58BR and KB-D12/02-58PEG are characterized by a plateau age of ~78 Ma and highly reduced incremental ages, far below the protolith cooling ages described above. Assuming that by stepwise heating Ar will be released from the muscovite rims first, this is a strong indication for lattice distortion and related Ar loss along the grain boundaries due to cataclastic shearing or alteration by hydrothermal fluids, and incomplete subsequent resetting of the Ar isotopic system. Studies from other fault zones (e.g., Müller et al. 2002) also considered this Ar loss to be related to weathering and weathering-related alteration of the samples or even to loss due to recoil during irradiation, particularly if the rims were damaged/deformed during the fault activity. The samples described in our study were all taken from drill cores, and the sampling sites are rather deep-seated compared to surface exposures. We therefore take our samples to be affected by long-term weathering at surface conditions only to a minor degree. A minimum age of ca. 43 Ma for shearing-related damage is suggested by the reduced incremental ages. As the incremental ages are in parts highly erratic, however, statements about the timing of shearing remain speculative.

Zircon fission track ages show a tendency of decreasing ages from protoliths toward the fault rocks, as indicated by reduced track lengths in zircons from cataclasites and fault gouges. The HR ages indicate cooling of the western part

of the Koralm Complex below the ZPAZ (approximately 300–200°C, cf. Wagner and Van den haute 1992) during Late Cretaceous times, i.e. between 77 and 65.5 Ma. In the more central parts cooling occurred slightly earlier (77.6 ± 5.5 Ma) (sample TB-D02/02-458) than along the western margin of the Koralm Massif (65.5–68 Ma, samples from KB-D12/02) (Fig. 6). ZFT ages of 68 and 64 Ma in the LFZ and related shear zones are slightly younger than in the HR, still within the 2σ error. In contrast to the AFT ages, ZFT single grain ages from the fault zone domains do not show clearly separated age populations, but fairly normal distributions (Figs. 6, 7). The chi-square test was passed in all zircon samples. The calculated central ages are therefore interpreted as cooling ages and are not evidence for the timing of a thermal event along the LFZ. Partial annealing may, however, be indicated by reduced track lengths within the cataclasite samples. The MTL shift from 10.13 ± 1.40 μm (sample 28DZ) and 10.24 ± 1.02 μm (sample 458DZ) to 7.13 ± 1.56 μm (sample 28 FC) and 8.22 ± 1.67 μm (sample 458FC) within a distance of 60 and 80 cm, respectively. By choosing a consistent etching time, the effects of anisotropic track annealing were avoided. We therefore suggest that secondary heating caused by a thermal event affected the ZFTs within the fault core cataclasites subsequent to the cooling of the adjacent protolith.

7.3 Gosau basin formation

In a regional geological context the evolution defined by the $^{40}Ar/^{39}Ar$ and ZFT ages coincides with the formation of the Gosau-type sedimentary basins (Fig. 2), which started during Santonian times (~85 Ma) and was characterized by a polyphase subsidence history (e.g., Willingshofer et al. 1999). Remnants of these basins are situated at the eastern and western margin of the Koralm Complex, the Gosau basins of Kainach and St. Paul, respectively (Fig. 2), and at the southwestern margin of the Saualm Complex (Krappfeld basin, Wilkens 1989). The Gosau basin of St. Paul is in close vicinity to the LFZ at the southern margin of the Saulam Complex (Fig. 2). Subsidence of the Gosau basins is closely related to the exhumation of the surrounding basement complexes (e.g., Neubauer et al. 1995; Kurz and Fritz 2003). Both basement domes and the related basins formed within a system of strike-slip and normal faults (Neubauer et al. 1995). As described by Wilkens (1989), the sedimentary sequence within the Gosau deposits is characterized by a well-developed angular and erosive unconformity at the Cretaceous/Palaeogene boundary (~65 Ma).

Although the $^{40}Ar/^{39}Ar$ muscovite ages and ZFT ages from fault-related cataclasites apparently coincide with distinct events within the Gosau basins, a clear thermochronological relationship to Late-Cretaceous to Palaeogene movement on the LFZ cannot be proven by our data. The younger ages obtained in the very first Ar release steps of some samples, as well as the slightly reduced zircon FT ages and reduced track lengths, could represent rejuvenation due to cataclastic shearing and/or alteration by hydrothermal fluids in the fault zones, but can certainly not be unequivocally established, since the observed temperatures within the LFZ were not high enough to reset both systems completely. These $^{40}Ar/^{39}Ar$ muscovite and ZFT ages therefore indicate that both thermochronological systems were partly thermally affected along the LFZ, most probably during Miocene times. Also, the cooling models (Fig. 9) provide no evidence for a difference in the cooling history across the LFZ during Late Cretaceous to Palaeogene times, which would have been evidence for differential vertical movement and therefore activity of the LFZ over this period.

Apatite fission track protolith ages indicate cooling of the Koralm Complex below the APAZ (120–60°C) between ~50 and ~30 Ma (Fig. 9). In the central part of the Koralm Complex the AFT ages are older (~51 Ma) than those found along the western margin (~36 to 43 Ma, Fig. 8), indicating the effect of elevation. Cooling below the APAZ occurred earlier in the central parts of the Koralm Massif than along the western margin. The sedimentary record within the Gosau basins west of the Koralm massif, mainly characterized by carbonate sequences abruptly cut by an erosive unconformity, is documented up to the Middle Eocene (Lutetian stage, approximately 45 Ma, see Wilkens 1989). Although the subsidence history of these basins during Palaeogene times is badly constrained, we infer that the evolution of the Gosau basins and the exhumation-related cooling of the Koralm massif were coupled processes up to Eocene times.

8 Conclusions

1. Exhumation and cooling of the Koralm massif from mid-crustal levels was mainly completed at the end of the Cretaceous, as indicated by $^{40}Ar/^{39}Ar$ white mica and ZFT ages from the Koralm basement (~80 to 65 Ma).
2. Ar release spectra from muscovites in cataclastic shear zones in part show highly reduced incremental ages, indicating lattice distortion or hydrothermal alteration, and incomplete subsequent resetting of the Ar isotopic system only for the first low-temperature steps.
3. Rejuvenation of ZFT ages along the LFZ indicates a thermal event. Recognition of a Cretaceous displacement event is hampered by the fact that the Cretaceous cooling is regionally very widespread. Additionally,

potential Late Cretaceous structural elements were frequently reactivated by faulting during Miocene times.

4. $^{40}Ar/^{39}Ar$ muscovite and ZFT ages from LFZ-related cataclasites do not bear clear evidence of pre-Miocene faulting. Rather, both thermochronological systems were partly thermally affected along the LFZ during Miocene times.
5. During the main phase of eastward extension-related displacement, Austroalpine crustal blocks in the eastern parts of the central Eastern Alps do not show significant differential exhumation.
6. The disintegration of the Styrian Basin and the separation of the Lavanttal Basin by the uplifting Koralm block is most probably related to vertical displacement along the LFZ around 12–10 Ma.

Acknowledgments This study has been carried out during a research project granted by the Austrian Science Fund (FWF project P-17697-N10). Statements and comments to a previous version of the manuscript by Marco G. Malusá, Annia Fayon, and Martin Danisík were a welcome contribution to improvement of the paper. We highly appreciate the formal reviews by Neil Mancktelow and an anonymous reviewer. Geoffrey Milnes is thanked for his editorial comments. We gratefully acknowledge the Österreichische Bundesbahnen (ÖBB) (division Infrastruktur Bau) and the 3G Gruppe Geotechnik Graz ZT GmbH for giving access to pilot tunnel excavations, drill core samples, borehole logs and geological maps acquired during the Koralm tunnel investigation campaign.

References

Barbarand, J., Hurford, T., & Carter, A. (2003). Variation in apatite fission-track length measurement: Implications for thermal history modelling. *Chemical Geology, 198*, 77–106.

Beck-Mannagetta, P. (1980). *Geologische Karte der Republik Österreich 1:50.000–188 (Wolfsberg)*. Vienna: Geologische Bundesanstalt.

Bigot-Cormier, F., Sosson, M., Poupeau, G., Stéphan, J. F., & Labrin, E. (2006). The denudation history of the Argentera Alpine External Massif (Western Alps, Franc-Italy): An overview from the analysis of fission tracks in apatites and zircons. *Geodinamica Acta, 19*, 455–473.

Bossé, V., Féraud, G., Ballévre, G., Peucat, J.-J., & Corsini, M. (2005). Rb-Sr and $^{40}Ar/^{39}Ar$ ages in blueschists from the Ile de Groix (Armorican Massif, France): Implications for closure mechanisms in isotopic systems. *Chemical Geology, 220*, 21–45.

Brandon, M. T., Roden-Tice, M. K., & Garver, J. I. (1998). Late Cenozoic exhumation of the Cascadia accretionary wedge in the Olympic Mountains, northwest Washington State. *Geological Society of America Bulletin, 110*, 985–1009.

Brodie, K., Fettes, D., Harte, B., & Schmid, R. (2002). *Structural terms including fault rock terms*. IUGS Subcommission on the Systematics of Metamorphic Rocks. *International Union of Geosciences.*

Brosch, F. J., & Kurz, W. (2008). Fault damage zones dominated by high-angle fractures within layer-parallel brittle shear zones: Examples from the Eastern Alps. *Geological Society of London Special Publication, 299*, 75–95.

Burtner, R. L., Nigrini, A., & Donelick, R. A. (1994). Thermochronology of Lower Cretaceous source rocks in the Idaho-Wyoming thrust belt. *American Association of Petroleum Geologists Bulletin, 78*, 1613–1636.

Caine, J. S., Evans, J. P., & Forster, C. B. (1996). Fault zone architecture and permeability structure. *Geology, 24*, 1025–1028.

Carlson, W. D., Donelick, R. A., & Ketcham, R. A. (1999). Variability of apatite fission-track annealing kinetics: Experimental results. *American Mineralogist, 84*, 1213–1223.

Chester, F. M., Evans, J. P., & Biegel, R. L. (1993). Internal structure and weakening mechanisms of the San Andreas. *Journal of Geophysical Research, 98*, 771–786.

Chopin, C., & Maluski, H. (1980). $^{40}Ar/^{39}Ar$ dating of high pressure metamorphic micas from the Gran Paradiso Area (Western Alps): Evidence against the blocking temperature concept. *Contributions to Mineralogy and Petrology, 74*, 109–122.

Cliff, R. A., Droop, G. T. R., & Rex, D. C. (1985). Alpine metamorphism in the south-east Tauern Window, Austria: II. Heating, cooling and uplift rates. *Journal of Metamorphic Geology, 3*, 403–415.

d'Alessio, M. A., Blythe, A. E., & Bürgmann, R. (2003). No frictional heat along the San Gabriel fault, California: Evidence from fission-track thermochronology. *Geology, 31*, 541–544.

Decker, K., Meschede, M., & Ring, U. (1993). Fault slip analysis along the northern margin of the Eastern Alps (Molasse, Helvetic nappes, North and South Penninic flysch, and Northern Calcareous Alps). *Tectonophysics, 223*, 291–312.

Decker, K., & Peresson, H. (1996). Tertiary kinematics in the Alpine-Carpathian-Pannonian system: Links between thrusting, transform faulting and crustal extension. In G. Wessely & W. Liebl (Eds.), *Oil and gas in alpidic thrustbelts and basins of Central and Eastern Europe* (pp. 69–77). Bath: EAGE Special Publication.

Dunkl, I. (2002). TRACKKEY: A windows program for calculation and graphical presentation of fission track data. *Computers and Geosciences, 28*, 3–12.

Dunkl, I., Kuhlemann, J., Reinecker, J., & Frisch, W. (2005). Cenozoic relief evolution of the Eastern Alps—Contraints from apatite fission track age-provenance of Neogene intramontane sediments. *Austrian Journal of Earth Sciences (Mitteilungen der Österreichischen Geologischen Gesellschaft), 98*, 92–105.

Dunlap, W. J. (1997). Neocrystallization or cooling? $^{40}Ar/^{39}Ar$ ages of white micas from low-grade mylonites. *Chemical Geology, 143*, 181–203.

Ebner, F., & Sachsenhofer, R. F. (1995). Paleogeography, subsidence and thermal history of the Neogene Styrian Basin (Pannonian basin system, Austria). *Tectonophysics, 242*, 133–150.

Farley, K. A. (2002). TRACKKEY: A windows program for calculation and graphical presentation of fission track data. *Computers and Geosciences, 28*, 3–12.

Faulkner, D. R., Jackson, C. A. L., Lunn, R. J., Schlische, R. W., Shipton, Z. K., Wibberley, C. A. J., et al. (2010). A review of recent developments concerning the structure, mechanics and fluid flow properties of fault zones. *Journal of Structural Geology, 32*, 1557–1575.

Faulkner, D. R., Lewis, A. C., & Rutter, E. H. (2003). On the internal structure and mechanics of large strike-slip fault zones: Field observations of the Carboneras fault in southeastern Spain. *Tectonophysics, 367*, 235–251.

Fodor, L., Gerdes, A., Dunkl, I., Koroknai, B., Pécskay, Z., Trajanova, M., et al. (2008). Miocene emplacement and rapid cooling of the Pohorje pluton at the Alpine-Pannonian-Dinaric junction: A geochronological and structural study. *Swiss Journal of Geosciences, 101*(Supplement 1), S255–S271.

Fodor, L., & POSIHU Research Group. (2003). Miocene exhumation of the Pohorje-Kozjak Mts., Slovenia (Alpine–Pannonian transition). *Geophysical Research Abstracts, 5*, 11814.

Freeman, S. R., Inger, S., Butler, W. H., & Cliff, R. A. (1997). Dating deformation using Rb-Sr in white mica: Greenschist facies deformation ages from the Entrelor shear zone, Italian Alps. *Tectonics, 16*, 57–76.

Frisch, W., Dunkl, I., & Kuhlemann, J. (2000). Post-collisional orogen-parallel large-scale extension in the Eastern Alps. *Tectonophysics, 327*, 239–265.

Frisch, W., Kuhlemann, J., Dunkl, I., & Brügel, A. (1998). Palinspastic reconstruction and topographic evolution of the Eastern Alps during late Tertiary tectonic extrusion. *Tectonophysics, 297*, 1–16.

Frost, E., Dolan, J., Sammis, C., Hacker, B., Cole, J., & Ratschbacher, L. (2009). Progressive strain localization in a major strike-slip fault exhumed from midseismic depths: Structural observations from the Salzach-Ennstal-Mariazell-Puchberg fault system, Austria. *Journal of Geophysical Research, 114*, B04406. doi: 10.1029/2008JB005763.

Fügenschuh, B., Mancktelow, N. S., & Seward, D. (2000). Cretaceous to Neogene cooling and exhumation history of the Oetztal-Stubai basement complex, eastern Alps. A structural and fission track study. *Tectonics, 19*, 905–918.

Fügenschuh, B., Seward, D., & Mancktelow, N. (1997). Exhumation in a convergent orogen: The western Tauern window. *Terra Nova, 9*, 213–217.

Galbraith, R. F. (1990). The radial plot: Graphical assessment of spread in ages. *Nuclear Tracks and Radiation Measurements, 17*, 207–214.

Genser, J., & Neubauer, F. (1989). Low angle normal faults at the eastern margin of the Tauern window (Eastern Alps). *Mitteilungen der Österreichischen Geologischen Gesellschaft, 81*, 233–243.

Gleadow, A. J. W., Hurford, A. J., & Quaife, R. D. (1976). Fission track dating of zircon: Improved etching techniques. *Earth and Planetary Science Letters, 33*, 273–276.

Glodny, J., Ring, U., & Kühn, A. (2008). Coeval high-pressure metamorphism, thrusting, strike-slip and extensional shearing in the Tauern Window, Eastern Alps. *Tectonics, 27*, TC4004. doi: 10.1029/2007TC002193.

Green, P. F., Duddy, I. R., Gleadow, A. J. W., Tingate, P. R., & Laslett, G. M. (1986). Thermal annealing of fission tracks in apatite 1. A qualitative description. *Chemical Geology, 59*, 237–253.

Hames, W. E., & Browning, S. A. (1994). An empirical evaluation of the argon diffusion geometry in muscovite. *Earth and Planetary Science Letters, 124*, 161–167.

Hames, W. E., & Cheney, J. T. (1997). On the loss of ^{40}Ar* from muscovite during polymetamorphism. *Geochimica and Cosmochimica Acta, 61*, 3863–3872.

Hammerschmidt, K., & Frank, E. (1991). Relics of high pressure metamorphism in the Lepontine Alps (Switzerland)—^{40}Ar/^{39}Ar and microprobe analyses on K-micas. *Schweizerische Mineralogische und Petrographische Mitteilungen, 71*, 261–274.

Handler, R., Neubauer, F., Velichkova, S. H., & Ivanov, Z. (2004). ^{40}Ar/^{39}Ar age constraints on the timing of magmatism and post-magmatic cooling in the Pnagyurishte region, Bulgaria. *Schweizerische Mineralogische und Petrographische Mitteilungen, 84*, 119–132.

Harer, G., & Otto, R. (2000). Koralmtunnel: Methodische Erkenntnisse aus der Projektvorbereitung. *Mitteilungen des Instituts für Angewandte Geowissenschaften BOKU, 10*, 27–42.

Hasabe, N., Tagami, T., & Nishimura, T. (1994). Towards zircon fission-track thermochronology: Reference framework for confined track length measurements. *Chemical Geology, 112*, 169–178.

Hejl, E. (1997). 'Cold spots' during the Cenozoic evolution of the Eastern Alps: Thermochronological interpretation of apatite fission-track data. *Tectonophysics, 272*, 159–173.

Hejl, E. (1998). Über die känozoische Abkühlung und Denudation der Zentralalpen östlich der Hohen Tauern—eine Apatit-Spaltspurenanalyse. *Mitteilungen der Österreichischen Geologischen Gesellschaft, 89*, 179–200.

Hurford, A. J., & Green, P. F. (1983). The zeta age calibration of fission-track dating. *Chemical Geology, 41*, 285–312.

Ketcham, R. A. (2005). Forward and inverse modeling of low-temperature thermochronometry data. *Reviews in Mineralogy and Geochemistry, 58*, 75–314.

Ketcham, R. A., Donelick, R. A., & Carlson, W. D. (1999). Variability of apatite fission-track annealing kinetics: III. Extrapolation to geological time scales. *American Mineralogist, 84*, 1235–1255.

Kirschner, D. L., Cosca, M. A., Masson, H., & Hunziker, J. C. (1996). Staircase ^{40}Ar/^{39}Ar spectra of fine-grained white mica: Timing and duration of deformation and empirical constraints on argon diffusion. *Geology, 24*, 747–751.

Kurz, W., & Fritz, H. (2003). Tectonometamorphic evolution of the Austroalpine Nappe Complex in the central Eastern Alps—Consequences for the Eo-Alpine evolution of the Eastern Alps. *International Geology Review, 45*, 1100–11127.

Kurz, W., Fritz, H., Piller, W. E., Neubauer, F., & Genser, J. (2001). Overview of the Paleogene of the Eastern Alps. In W. E. Piller & M. Rasser (Eds.), *Paleogene of the Eastern Alps* (Vol. 14, pp. 11–56). Vienna: Österreichische Akademie der Wissenschaften, Schriftenreihe der Erdwisseschaftichen Kommission.

Kurz, W., Handler, R., & Bertholdi, C. (2008). Tracing the exhumation of the Eclogite Zone (Tauern Window, Eastern Alps) by ^{40}Ar/^{39}Ar dating of white mica in eclogites. *Swiss Journal of Geosciences, 101*(Supplement 1), S191–S206.

Laslett, G. M., Green, P. F., Duddy, I. R., & Gleadow, A. J. W. (1987). Thermal annealing of fission tracks in apatite 2: A quantitative analysis. *Chemical Geology, 65*, 1–13.

Lenhardt, W. A., Freudenthaler, C., Lippitsch, R., & Fiegweil, E. (2007). Focal-depth distributions in the Austrian Eastern Alps based on macroseismic data. *Austrian Journal of Earth Sciences (Mitteilungen der Österreichischen Geologischen Gesellschaft), 100*, 66–79.

Linzer, H.-G., Decker, K., Peresson, H., Dell′Mour, R., & Frisch, W. (2002). Balancing lateral orogenic float of the Eastern Alps. *Tectonophysics, 354*, 211–237.

Lips, A. L. W., White, S. H., & Wijbrans, J. R. (1998). ^{40}Ar/^{39}Ar laserprobe direct dating of discrete deformational events: A continous record of early Alpine tectonics in the Pelagonian Zone, NW Aegean area, Greece. *Tectonophysics, 298*, 133–153.

Maddock, R. H. (1983). Melt origin of fault-generated pseudotachylites demonstrated by textures. *Geology, 11*, 105–108.

Malusá, M. G., Philippot, P., Zattin, M., & Martin, S. (2006). Late stages of exhumation constrained by structural, fluid inclusion and fission track analyses (Sesia-Lanzo unit, Western European Alps). *Earth and Planetary Science Letters, 243*, 565–580.

Malusá, M. G., Polino, R., Zattin, M., Bigazzi, G., Martin, S., & Piana, F. (2005). Miocene to Present differential exhumation in the Western Alps: Insights from fission track thermochronology. *Tectonics, 24*, 2004TC001782.

Malusá, M. G., Zattin, M., Andó, S., Garzanti, E., & Vezzoli, G. (2009). Focused erosion in the Alps constrained by fission-track ages on detrital apatites. *Geological Society of London Special Publication, 324*, 141–152.

Mancktelow, N. S., Stöckli, D. F., Grollimund, B., Müller, W., Fügenschuh, B., Viola, G., et al. (2001). The DAV and

Periadriatic fault systems in the Eastern Alps south of the Tauern Window. *International Journal of Earth Sciences, 90*, 593–622.

Müller, W., Dallmeyer, R. D., Neubauer, F., & Thöni, M. (1999). Deformation-induced resetting of Rb/Sr and $^{40}Ar/^{39}Ar$ mineral systems in a low-grade, polymetamorphic terrane (Eastern Alps, Austria). *Journal of the Geological Society of London, 156*, 261–278.

Müller, W., Kelley, S. P., & Villa, I. M. (2002). Dating fault-generated pseudotachylites: Comparison of 40Ar/39Ar stepwise-heating, laser-ablation and Rb-Sr microsampling analyses. *Contributions to Mineralogy and Petrology, 144*, 57–77.

Müller, W., Mancktelow, N. S., & Meier, M. (2000). Rb-Sr microchrons of synkinematic mica in mylonites: An example from the DAV fault of the Eastern Alps. *Earth and Planetary Science Letters, 180*, 385–397.

Müller, W., Prosser, G., Mancktelow, N. S., Villa, I. M., Kelley, S. P., Viola, G., et al. (2001). Geochronological constraints on the evolution of the Periadriatic Fault System (Alps). *International Journal of Earth Sciences, 90*, 623–653.

Murakami, M., Tagami, T., & Hasabe, N. (2002). Ancient thermal anomaly of an active fault system: Zircon fission-track evidence from Nojima GSJ 750 m borehole samples. *Geophysical Research Letters, 29*, 2123. doi:10.1029/2002GL015679.

Murakami, M., Yamada, R., & Tagami, T. (2006). Short-term annealing characteristics of spontaneous fission tracks in zircon. *Chemical Geology, 227*, 214–222.

Nebert, K. (1983). Zyklische Gliederung der Eibiswalder Schichten. *Jahrbuch der Geologischen Bundesanstalt, 126*, 259–285.

Neubauer, F., Dallmeyer, R. D., Dunkl, I., & Schirnik, D. (1995). Late Cretaceous exhumation of the metamorphic Gleinalm dome, Eastern Alps: Kinematics, cooling history and sedimentary response in a sinistral wrench corridor. *Tectonophysics, 242*, 79–98.

Neubauer, F., Fritz, H., Genser, J., Kurz, W., Nemes, F., Wallbrecher, E., et al. (2000). Structural evolution within an extruding block: Model and application to the Alpine-Pannonian system. In F. K. Lehner & J. L. Urai (Eds.), *Aspects of tectonic faulting* (pp. 141–154). Berlin: Springer.

Neubauer, F., & Genser, J. (1990). Architektur und Kinematik der östlichen Zentralalpen—eine Übersicht. *Mitteilungen des Naturwissenschaftlichen Vereins für Steiermark, 120*, 203–219.

Otsuki, K., Monzawa, N., & Nagase, T. (2003). Fluidization and melting of fault gouge during seismic slip: Identification in the Nojima fault zone and implications for focal earthquake mechanisms. *Journal of Geophysical Research, 108*, 2001JB1711.

Peresson, H., & Decker, K. (1997). Far-field effects of Late Miocene subduction in the Eastern Carpathians: E-W compression and inversion of structures in the Alpine-Carpathian-Pannonian region. *Tectonics, 16*, 38–56.

Piller, W. E., et al. (2004). Die Stratigraphische Tabelle von Österreich 2004 (sedimentäre Schichtfolgen). Wien: Österreichische stratigraphische Kommission und Kommission für die paläontologische und stratigraphische Erforschung Österreichs der Österreichischen Akademie der Wissenschaften.

Piller, W., & Harzhauser, M. (2005). The myth of the brackish Sarmatian Sea. *Terra Nova, 17*, 1–6.

Pischinger, G., Kurz, W., Übleis, M., Egger, M., Fritz, H., Brosch, F. J., et al. (2008). Fault slip analysis in the Koralm Massif (Eastern Alps) and consequences for the final uplift of "cold spots" in Miocene times. *Swiss Journal of Geosciences, 101*(Supplement 1), S235–S254.

Puch, T. (1995). Spaltspurendatierungen an Apatit und Zirkon als tracer tektonischer Prozesse im Bereich Koralpe-Saualpe-Krappfeld (Kärnten/Österreich), Ostalpen. Unpublished Diploma thesis, Naturwissenschaftliche Fakultät, Universität Graz, pp. III + 124 pp.

Rabitsch, R., Wölfler, A., & Kurz, W. (2007). Fission track dating in fault zones: an example from the Eastern Alps. *Geophysical Research Abstracts, 9*, EGU2007-A-02732.

Rahn, M. K., Brandon, M. T., Batt, G. E., & Garver, J. I. (2004). A zero-damage model for fission-track annealing in zircon. *American Mineralogist, 89*, 473–484.

Ratschbacher, L., Frisch, W., Linzer, H.-G., & Merle, O. (1991). Lateral extrusion in the Eastern Alps. Part 2: Structural analysis. *Tectonics, 10*, 257–271.

Reddy, S. M., Cliff, R. A., & East, R. (1993). Thermal history of the Sonnblick Dome, south-east Tauern Window, Austria: Implications for Heterogenous uplift within the Pennine basement. *Geologische Rundschau, 82*, 667–675.

Reinecker, J. (2000). Stress and deformation: Miocene to present-day tectonics in the Eastern Alps. *Tübinger Geowissenschaftliche Arbeiten, Serie A, 55*, 128.

Reinecker, J., & Lenhardt, W. A. (1999). Present-day stress field and deformation in eastern Austria. *Geologische Rundschau, 88*, 532–550.

Reischenbacher, D., Rifelj, H., Sachsenhofer, R., Jelen, B., Coric, S., Gross, M., et al. (2007). Early Badenian paleoenvironment in the Lavanttal Basin (Mühldorf Formation; Austria): Evidence from geochemistry and paleontology. *Austrian Journal of Earth Sciences, 100*, 202–229.

Reischenbacher, D., & Sachsenhofer, R. F. (2008). Eine interdisziplinäre Betrachtung des Lavanttaler Beckens. *Journal of Alpine Geology, 49*, 86–87.

Sachsenhofer, R. (1996). The Neogene Styrian Basin: An overview. *Mitteilungen der Gesellschaft der Geolgie- und Bergbaustudenten Österreichs, 41*, 19–32.

Sachsenhofer, R. F., Dunkl, I., Hasenhüttl, C., & Jelen, B. (1998). Miocene thermal history of the southwestern margin of the Styrian Basin: Vitrinite reflectance and fission-track data from the Pohorje/Kozjak area (Slovenia). *Tectonophysics, 297*, 17–29.

Sachsenhofer, R. F., Jelen, B., Hasenhüttl, C., Dunkl, I., & Rainer, T. (2001). Thermal history of tertiary basins in Slovenia (Alpine-Dinaride-Pannonian junction). *Tectonophysics, 334*, 77–99.

Sachsenhofer, R. F., Kogler, A., Polesny, H., Strauss, P., & Wagreich, M. (2000). The Neogene Fohnsdorf Basin: Basin formation and basin inversion during lateral extrusion in the Eastern Alps (Austria). *Geologische Rundschau, 89*, 415–430.

Sachsenhofer, R. F., Lankreijer, A., Cloething, S., & Ebner, F. (1997). Subsidence analysis and quantitative basin modelling in the Styrian Basin (Pannonian Basin System, Austria). *Tectonophysics, 272*, 175–196.

Selverstone, J. (1988). Evidence for east-west crustal extension in the Eastern Alps: Implications for the unroofing history of the Tauern window. *Tectonics, 7*, 87–105.

Siebel, W., Hann, H. P., Danisík, M., Shang, C. K., Berthold, C., Rohrmüller, J., et al. (2010). Age constraints on faulting and fault reactivation. *International Journal of Earth Sciences, 99*, 1187–1197.

Spiegel, C., Kuhlemann, J., & Frisch, W. (2007). Tracing sediment pathways by zircon fission track analysis: Oligocene marine connections in Central Europe. *International Journal of Earth Sciences, 96*, 363–374.

Steidl, A., Goricki, A., Schubert, W., & Riedmüller, G. (2001). Geological and geotechnical ground characterisation for the Koralm Tunnel Route selection. *Felsbau, 19*, 14–21.

Tagami, T., & Murakami, M. (2007). Probing fault zone heterogeneity on the Nojima fault: Constraints from fission-track analysis of borehole samples. *Tectonophysics, 443*, 139–152.

Tagami, T., & Shimada, C. (1996). Natural long-term annealing of the zircon fission track system around a granitic pluton. *Journal of Geophysical Research, 101*, 8245–8255.

Thöni, M., & Miller, Ch. (1996). Garnet Sm-Nd data from the Saualpe and Koralpe (Eastern Alps, Austria): Chronological and P-T constraints on the thermal and tectonic history. *Journal of Metamorphic Geology, 14*, 453–466.

Vavrovsky, G. M., Schneider, K. M., & Harer, G. (2001). Koralmbahn—A new railway line in Southern Austria. *Felsbau, 19*, 8–12.

Villa, I. M. (1998). Isotopic closure. *Terra Nova, 10*, 42–47.

von Blanckenburg, F., & Villa, I. M. (1988). Argon retentivity and argon excess in amphiboles from the garbenschists of the Western Tauern Window, Eastern Alps. *Contributions to Mineralogy and Petrology, 100*, 1–11.

von Blanckenburg, F., Villa, I. M., Baur, H., Morteani, G., & Steiger, R. H. (1989). Time calibration of a PT-path from the Western Tauern Window, Eastern Alps: The problem of closure temperatures. *Contributions to Mineralogy and Petrology, 101*, 1–11.

Wagner, G. A., & Van den haute, P. (1992). *Fission-track dating* (285 pp). Stuttgart: Enke.

Wagreich, M., & Schmid, H. P. (2002). Backstripping dip-slip fault histories: Apparent slip rates for the Miocene of the Vienna Basin. *Terra Nova, 14*, 163–168.

Wiesinger, M., Neubauer, F., & Handler, R. (2006). Exhumation of the Saualpe eclogite unit, Eastern Alps: Constraints from $^{40}Ar/^{39}Ar$ ages and structural investigations. *Mineralogy and Petrology, 88*, 149–180.

Wilkens, E. (1989). Paläogene Sedimente des Krappfeldes und seiner Umgebung. In T. Appold & F. Thiedig (Eds.), *Arbeitstagung der Geologischen Bundesanstalt* (pp. 85–99). Vienna: Geologische Bundesanstalt.

Willingshofer, E., Neubauer, F., & Cloething, S. (1999). The significance of Gosau-type basins for the Late Cretaceous tectonic history of the Alpine-Carpathian belt. *Physics and Chemistry of the Earth, 24*, 687–695.

Wolf, R. A., Farley, K. A., & Kass, D. M. (1998). Modeling the temperature sensitivity of the apatite (U-Th)/He thermochronometer. *Chemical Geology, 148*, 105–114.

Wölfler, A., Dekant, C., Danišík, M., Kurz, W., Dunkl, I., Putiš, M., et al. (2008). Late stage differential exhumation of crustal blocks in the central Eastern Alps: Evidence from fission track and (U-Th)/He thermochronology. *Terra Nova, 20*, 378–384.

Wölfler, A., Kurz, W., Danisik, M., & Rabitsch, R. (2010). Dating of fault zone activity by apatite fission track and apatite (U-Th)/He thermochronometry: A case study from the Lavanttal fault system (Eastern Alps). *Terra Nova, 22*, 274–282.

Zaun, P. E., & Wagner, G. A. (1985). Fission-track stability in zircon under geological conditions. *Nuclear Tracks and Radiation Measurements, 10*, 303–307.

Zwingmann, H., & Mancktelow, N. (2004). Timing of Alpine fault gouges. *Earth and Planetary Science Letters, 223*, 415–425.